Chapter 4

Cygnus X-1 Inclination from Polarimetry

4.1 Introduction

Masses are difficult to measure accurately, because most methods are only generally applicable to binary systems. Astrometric motion of binaries can be fit to Kepler's laws to determine component masses. However, many systems orbit too closely, or are too distant from Earth, for their astrometric motion to be resolved. The radial velocity technique is used to determine line of sight motion of luminous sources, and orbital parameters such as period and eccentricity can be determined to exquisite precision. However, since this technique is blind to motion in the plane of the sky, and hence to orbital inclination, masses determined from this technique are only lower limits. Statistical analyses can be applied to large samples of objects, such as extrasolar planets, to estimate the true distribution of masses. But masses of individual objects obtained by the radial velocity technique can be very imprecise.

Since polarization is a geometry-dependent effect, one might expect that it can be used to constrain orbital inclination of binary systems. In particular, polarimetry holds promise for determining masses in high mass X-ray binaries. These systems consist of an OB supergiant and black hole, the prototype of which is Cygnus X-1. The $40 \pm 10\ M_{\odot}$ (Ziólkowski 2005), O9.7Iab supergiant in this system (Walborn 1973) nearly fills its Roche lobe, and the $13.5 - 29\ M_{\odot}$ black hole (Ziólkowski 2005) accretes matter partly from a focused stellar wind (Gies & Bolton 1986b) as well as occasional Roche lobe overflow. Tighter constraints on the mass of the Cygnus X-1 black hole are necessary to test stellar evolution models and study general relativity on finer scales.

4.2 Overview of Cygnus X-1

4.2.1 Accretion

Cygnus X-1 harbors an accretion disk, which is evident by its X-ray luminosity of $(2 - 5.5) \times 10^{37}$ erg/s (Syunyaev & Trümper 1979, Dolan et al. 1979, Balucinska-Church et al. 2000) and significant emission of gamma rays (Albert et al. 2007). Its X-ray spectrum is composed of blackbody and power law components. The blackbody component of the spectrum comes from the accretion disk, where $kT \approx 0.1$ keV and the disk luminosity is 4.7×10^{36} erg/s (Balucinska-Church et al. 1995). The power law component, with flux $F(E) \propto E^{-\Gamma}$, is generated by Compton scattering of disk emission by either a hot corona of electrons (Shapiro et al. 1976) or at the base of a jet (Brocksopp et al. 1999a).

Stirling et al. (2001) observed a highly collimated (opening angle of < 2 degree), relativistic ($v/c \geq 0.6$) jet of ≈ 30 AU in length with the VLBA. Such a jet has been confirmed by Gallo et al. (2005) and Fender et al. (2006), and it points toward a nebula that Gallo et al. (2005) discovered in both the radio and the optical. Since the proper motion of Cygnus X-1 is perpendicular to the jet, the binary has never been at the center of the nebula. Therefore, the nebula is not a supernova remnant from the formation of the black hole; rather, it is interpreted as a bow shock between the remnants of the jet and the ISM. The kinetic energy of the jet and assumed counterjet represents 30% to 100% of the bolometric X-ray luminosity of Cygnus X-1 (Gallo et al. 2005, Russell et al. 2007). Thus, it appears that the energy of accretion is partitioned roughly equally between the jet and radiation.

The X-ray luminosity occasionally transitions from the fiducial, "low/hard" state to the "high/soft state". The low/hard state dominates the duty cycle: Cygnus X-1 is in this state about 90% of the time (Gallo et al. 2005). In the low/hard state, the relatively low accretion rate generates relatively low X-ray luminosity. The accretion rate is of order

$$\dot{m} \approx 0.1 \dot{M}_{\rm Edd} \tag{4.1a}$$

$$\dot{M}_{\rm Edd} = \frac{L_{\rm Edd}}{0.1c^2} \tag{4.1b}$$

$$L_{\rm Edd} \equiv \frac{4\pi G M m_p c}{\sigma_T} \tag{4.1c}$$

where $\dot{M}_{\rm Edd}$ is the Eddington accretion rate for 10% efficiency and $L_{\rm Edd}$ is the Eddington luminosity. The black hole mass is M, m_p is the mass of a proton, and σ_T is the Thomson scattering cross section for the electron. The low accretion rate in the low/hard state allows the optically thick, but geometrically thin, disk to be evaporated more efficiently. This causes the disk inner radius to retreat to $r_{\rm in} > 100R_s$, where $R_s \equiv 2GM/c^2$ is the Schwarzschild radius. An optically thin, hot corona of electrons flows from the disk inner radius to the event horizon. This corona generates the Comptonized power law, of photon index $\Gamma \approx 1.5$, that dominates the low/hard spectrum (Esin et al. 1998).

Occasionally, the mass accretion rate slightly increases, by only $\approx 15\%$ (Esin et al. 1998), which causes an increase in X-ray luminosity of about 10% to 20% (Brocksopp et al. 1999a). Evaporation of the disk proceeds less efficiently in the high/soft state, and the disk inner radius advances to the last stable orbit of the black hole, $r_{\rm in} = 3R_s$. This causes the disk blackbody emission to dominate over the power law from the corona (Esin et al. 1998). Exactly how disk accretion rate is tied to supergiant mass loss is debated, however.

The characteristic P Cygni profile observed in Hα from the supergiant indicates mass loss in the form of a stellar wind (Ninkov et al. 1987b). Since stellar wind from an OB supergiant issues roughly isotropically, atoms flowing towards the observer will have blueshifted absorption. Conversely, atoms flowing away from the observer will emit redshifted radiation. In the presence of the black hole, however, the distorted equipotential surface of the system will focus the stellar wind through the L1 point (Friend & Castor 1982, Gies & Bolton 1986b). Indeed, Miller et al. (2005) see evidence for such a wind from Chandra X-ray spectroscopy. The wind forms an accretion disk around the black hole. Intuitively, one would expect that increased mass loss from the supergiant would lead to increased accretion onto the black hole. However, the interaction of the radiatively-driven stellar wind and the X-ray luminosity of the accretion disk complicates matters.

Line radiation from the supergiant imparts momentum to absorbing atoms in the photosphere, which can accelerate the atoms past the supergiant's escape velocity to form a radiatively-driven wind (Castor et al. 1975). X-ray photoionization of atoms in this wind by the accretion disk will dramatically slow the wind, because the loss of electrons decreases the total force that stellar radiation can impart to the wind atoms. Increased stellar mass loss will form a denser wind, which will not be photoionized as completely. Thus, the mean wind speed will be increased. Since accretion rate

is given by $\dot{m} \propto \dot{M} v^{-4}$, where $\dot{M}$ is mass loss and v is flow velocity (Bondi & Hoyle 1944), a faster wind causes a lower accretion rate, even in the presence of increased stellar mass loss (Ho & Arons 1987, Stevens 1991). In contrast, wind density will be lower for decreased supergiant mass loss. X-ray ionization of the wind will be more complete, so there will exist fewer available lines for wind atoms to absorb. The slower wind will be accreted more readily than the faster wind. Therefore, decreased mass loss by the supergiant actually translates to a higher accretion rate by the black hole.

Gies et al. (2003, hereafter G03) observe a decrease in Hα equivalent width, and therefore strength of mass loss, during an X-ray flare. The time lag between these two events is small compared to the ten hour timescale for the wind to traverse the region between binary components, which indicates any lag is related to light travel time. They argue that the ionization of the supergiant's photosphere inhibits generation of a stellar wind, because wind velocity is lower than the escape velocity. This results in weak mass loss. However, they observe departures from such a simple model where mass loss is anticorrelated with X-ray flux.

Large changes in Hα emission have been observed by G03 while X-ray flux is constant. They also observe large variations in redshifted Hα emission even during inferior conjunction of the black hole (phase 0.5). At this phase, the Hα observed flows away from the black hole and is shadowed from X-rays by the primary. This gas does indeed lie in the X-ray shadow because similar Hα strength is observed during both low/hard and high/soft states, where X-ray luminosity changes. G03 calculate supergiant mass loss to be $(2.57 \pm 0.05) \times 10^{-6}\ M_{\odot}$/yr during the low/hard state, where X-ray flux is decreased. Mass loss in the presence of increased X-ray emission during the high/soft state appears to be only $(2.00 \pm 0.03) \times 10^{-6}\ M_{\odot}$/yr, which supports the hypothesis that increased accretion onto the black hole is actually produced by decreased mass loss by the supergiant.

4.2.2 Periodicities

The 5.6 day orbital period of Cygnus X-1 (Webster & Murdin 1972, Bolton 1972) is mirrored by ellipsoidal light modulation, where the tidally distorted, $V \approx 9$ supergiant fluctuates with amplitude $\Delta V \approx 0.04$ mag at twice the orbital frequency due to its time-variable cross-sectional area (Walker 1972; Lyutyj et al. 1973; Lester et al. 1973; Bochkarev et al. 1975; Bruevich et al. 1978; Balog et al. 1981; Gies & Bolton 1982; Khaliullina & Khaliullin 1981; Kemp et al. 1987; Ninkov et al. 1987a,

b; Voloshina et al. 1997; Brocksopp et al. 1999b). In addition to photometric observations in the optical, such second harmonic modulation has been observed in X-rays (Holt et al. 1976, Holt et al. 1979, Priedhorsky et al. 1995, Zhang et al. 1996, Paciesas et al. 1997, Pooley et al. 1999, Brocksopp et al. 1999a, Wen et al. 1999, Kitamoto et al. 2000, Manchanda 2001, Özdemir & Demircan 2001, Lachowicz et al. 2006, Poutanen et al. 2008), ultraviolet (Wolinski et al. 1996, Brocksopp et al. 1999a), near-IR (Leahy & Ananth 1992, Nadzhip et al. 1996, Brocksopp et al. 1999a), and radio (Pooley et al. 1999, Brocksopp et al. 1999a, Lachowicz et al. 2006).

There is also weak evidence for 39- and 78-day periods of unknown origin in ultraviolet and X-ray photometry (Kemp et al. 1978b), optical photometry (Karitskaya 1979, Lyutyi 1985, Kemp et al. 1987), and optical polarimetry (Kemp et al. 1978b). Kemp et al. (1978b) do not observe optical variability with these periods, and Dolan et al. (1979) do not observe X-ray variability. Therefore, it is unclear whether these periods are actually present.

Finally, there appears to be a longer period in the system, which is thought to originate from an oblique accretion disk that precesses due to gravitational torques from the supergiant. Previous observations imply a 294 day period from X-ray data (Metzger & Dolan 1968, Priedhorsky & Terrell 1982, Manchanda 1983, Priedhorsky et al. 1983), optical measurements (Karitskaya 1979, Kemp 1983, Kemp et al. 1983, Kemp et al. 1987), and ultraviolet/optical polarimetry (Kemp et al. 1983). However, more recent research suggests a 150 day period from X-ray (Pooley et al. 1999, Brocksopp et al. 1999a, Kitamoto et al. 2000, Özdemir & Demircan 2001, Lachowicz et al. 2006, Ibragimov et al. 2007, Poutanen et al. 2008), ultraviolet (Brocksopp et al. 1999a), optical (Brocksopp et al. 1999a, G03) and radio observations (Pooley et al. 1999, Brocksopp et al. 1999a, Lachowicz et al. 2006, Ibragimov et al. 2007, Poutanen et al. 2008). It has been suggested that the 294 day period is just aliasing of the "true" 150 day period, and that it is therefore not a real effect (Özdemir & Demircan 2001).

However, Kemp et al. (1983) saw a weaker 147 day period in addition to their 294 day period, and the 294 day period was observed through ≈ 15 cycles. Lachowicz et al. (2006, hereafter L06) see weak evidence for a current 293 day period in radio data, and they find a weak 150 day period to be present in the old data of Priedhorsky et al. (1983). L06 have studied archival data from the X-ray satellite Ariel 5 between 1976 and 2003, and they see a consistent, 150 day period throughout this time span. They further observe that the phase of precession has stayed roughly constant over

those ≈ 65 precessional periods. Additionally, using archival data from the Vela 5B satellite from 1969 to 1979, L06 see the existence of the 294 day period but not the 150 day period. Therefore, L06 suggest that the dominant period of disk precession physically evolved from the 294 day period to its second harmonic around 1980.

4.2.3 Polarization

The Cygnus X-1 system exhibits strong linear polarization in the optical with mean polarization $P_{\rm lin} \approx 5\%$. The optical (Gehrels 1972, Wolinski et al. 1996) and near-IR spectrum of polarization (Wilking et al. 1980) is consistent with the empirical interstellar polarization relation of Serkowski et al. (1975) as modified by Wilking et al. (1980). Since Cynus X-1 is 2.2 ± 0.2 kpc distant (Ziólkowski 2005) and in the plane of the galaxy, such strong interstellar polarization is almost unavoidable (Mathewson & Ford 1970, Barrett 1996, Fosalba et al. 2002). The position angle of net polarization changes by $\Delta\Theta(\lambda) = 0.8^\circ$ between U and V bands, which is significant at the 3σ level (Kemp et al. 1976).

Dolan & Tapia (1989) reject the hypothesis of constant position angle with wavelength at the 1% level of significance, and Wolinski et al. (1996) also observe the change in position angle. In addition, they observe wavelength-dependent Rayleigh scattering in the system as well as polarization in the ultraviolet larger than expected from interstellar polarization (section 4.5.5). Finally, the linear polarization of Cygnus X-1 is partly phase-locked to the first and second harmonic of the orbital frequency with amplitude $\Delta P_{\rm lin} \approx 0.2\%$ (Nolt et al. 1975; Kemp et al. 1978a, 1979; Kemp 1980a, Dolan & Tapia 1989; Wolinski et al. 1996; Nagae et al. 2008). These results imply that the linear polarization of Cygnus X-1 consists of interstellar and intrinsic components.

In addition to possessing strong linear polarization, Cygnus X-1 also harbors nonzero circular polarization of $P_{\rm circ} \approx 0.05\%$ (Michalsky et al. 1975a, b; Severny & Kuvshinov 1975; Michalsky & Swedlund 1977). The sense of circular polarization changes sign near the wavelength of peak linear polarization, which is consistent with interstellar origin (Martin 1974). Indeed, comparable circular polarization is observed in HD 204827, which is near Cygnus X-1 in the plane of the sky (Serkowski et al. 1975). Additionally, rotation of interstellar grain alignment along the line of sight to the system converts linear polarization to circular polarization with $\approx 1\%$ efficiency (Martin 1974,

Avery et al. 1975), which can account for the mean circular polarization of Cygnus X-1. Indeed, a change in grain size in addition to orientation along the line of sight produces a change in position angle with wavelength, which has been observed above.

However, in addition to variable linear polarization, circular polarization from Cygnus X-1 has also been observed to be variable (Michalsky et al. 1975b, Michalsky & Swedlund 1977). The B band amplitude of $\Delta P_{\rm circ} \approx 0.05\%$, were it caused by interstellar conversion of the variable linear polarization, would require the linear polarization to be variable at the $\Delta P_{\rm lin} \approx 5\%$ level. Since this is an order of magnitude larger than the observed $\Delta P_{\rm lin} \approx 0.2\%$, the circular polarization of Cygnus X-1 must consist of interstellar and intrinsic components. The dominant period of circular polarization has been observed to change from 2.8 days to 5.6 days over the course of eleven months (Michalsky & Swedlund 1977).

Gnedin et al. (2003, hereafter Gn03) suggest that a magnetic field origin for the intrinsic circular polarization of Cygnus X-1 implies a magnetic field at the last stable orbit of the black hole ($r_0 \equiv 3R_s$) of $B(r_0) = 10^7 - 10^8$ G. Long et al. (1980) observe linear polarization of X-rays to be $2.4 \pm 1.1\%$ at 2.6 keV and $5.3 \pm 2.5\%$ at 5.2 keV. Gn03 admit that the statistical significance of these detections is low, but they suggest that the decrease in X-ray polarization at lower energies may be due to Faraday depolarization. Faraday depolarization is the decrease in net polarization due to volume-integrated Faraday rotation (rotation of the plane of polarization due to a magnetic field). From Gnedin & Silant'ev (1980), the angle of Faraday rotation, χ_F, is

$$\chi_F \approx 0.6 \tau_T \left(\frac{B}{10^6 \text{ G}} \right) \left(\frac{1 \text{ keV}}{E} \right)^2 \cos\theta. \tag{4.2}$$

Here, θ is the angle between the local magnetic field and radiation propagation, and τ_T is the optical depth to Thomson scattering of the region. Assuming the difference in polarization between 2.6 keV and 5.3 keV is real, Gn03 calculate a magnetic field of $B(r_0) \geq 3 \times 10^7$ G. Furthermore, Gn03 suggest that Faraday depolarization of optical polarization implies $B(r_0) \approx 10^7$ G for a dipolar magnetic field. Thus, estimates of the strength of the magnetic field in the vicinity of the black hole, due to optical circular polarization as well as Faraday depolarization in the optical and in X-rays, imply a magnetic field of order $B(r_0) = 10^7 - 10^8$ G.

4.3 Inclination from Polarimetry

4.3.1 BME Scattering Model

The standard technique for inclination inversion from polarimetric observations comes from the theory of Brown et al. (1978, hereafter BME). An optically thin envelope of arbitrary distribution around one, or both, components in a binary with zero eccentricity is assumed. As long as the envelope is corotating and phase locked to the binary, polarimetric modulation of Thomson or Rayleigh scattered flux will be dependent on orbital inclination. For an envelope symmetric with respect to the orbital plane, BME note that polarimetric modulation will occur at the second harmonic of the orbital frequency. Asymmetry in the envelope will generate a first harmonic component.

From Aspin et al. (1981),

$$Q(\lambda) = \tau_0 \left[\gamma_1 \sin 2i \cos\lambda - \gamma_2 \sin 2i \sin\lambda - \left(1+\cos^2 i\right)\gamma_3 \cos 2\lambda + \left(1+\cos^2 i\right)\gamma_4 \sin 2\lambda\right] \tag{4.3a}$$

$$U(\lambda) = 2\tau_0 \left[\gamma_1 \sin i \sin\lambda + \gamma_2 \sin i \cos\lambda - \gamma_3 \cos i \sin 2\lambda - \gamma_4 \cos i \cos 2\lambda\right] \tag{4.3b}$$

$$\tau_0 \equiv \frac{\sigma_0}{2} \sum_{j=1}^{2} \iiint n(r,\theta,\phi) \sin\theta_j dr_j d\theta_j d\phi_j \tag{4.3c}$$

$$\tau_0\gamma_1 \equiv \frac{\sigma_0}{2} \sum_{j=1}^{2} f_j \iiint n(r,\theta,\phi) \sin 2\theta_j \cos\phi_j dr_j d\theta_j d\phi_j \tag{4.3d}$$

$$\tau_0\gamma_2 \equiv \frac{\sigma_0}{2} \sum_{j=1}^{2} f_j \iiint n(r,\theta,\phi) \sin 2\theta_j \sin\phi_j dr_j d\theta_j d\phi_j \tag{4.3e}$$

$$\tau_0\gamma_3 \equiv \frac{\sigma_0}{2} \sum_{j=1}^{2} f_j \iiint n(r,\theta,\phi) \sin^2\theta_j \cos 2\phi_j dr_j d\theta_j d\phi_j \tag{4.3f}$$

$$\tau_0\gamma_4 \equiv \frac{\sigma_0}{2} \sum_{j=1}^{2} f_j \iiint n(r,\theta,\phi) \sin^2\theta_j \sin 2\phi_j dr_j d\theta_j d\phi_j . \tag{4.3g}$$

Here, $\lambda = 2\pi\phi$ is the orbital longitude for zero eccentricity, ϕ is orbital phase, and $\sigma_0 \equiv 3\sigma_T/(16\pi)$. Spherical coordinates are in the reference frame of the binary, where $\theta = 0$ is perpendicular to the orbital plane. Summation progresses over stars $j = 1, 2$ in the binary, and f_j is the fractional luminosity of star j with respect to the system's flux. Regardless of the distribution of scatterers $n(r,\theta,\phi)$ and the intensity of each star, polarimetric modulation will occur at the fundamental and second harmonics of the orbital frequency.

Observed modulations in normalized Stokes parameters Q and U are decomposed into Fourier components according to

$$Q(\lambda) = q_0 + q_1 \cos\lambda + q_2 \sin\lambda + q_3 \cos 2\lambda + q_4 \sin 2\lambda \tag{4.4a}$$

$$U(\lambda) = u_0 + u_1 \cos\lambda + u_2 \sin\lambda + u_3 \cos 2\lambda + u_4 \sin 2\lambda. \tag{4.4b}$$

Note that observed Stokes parameters Q and U are normalized by stellar intensity. Terms of third order in orbital frequency are expected for non-zero eccentricity. It is generally accepted that the eccentricity of Cygnus X-1 is zero (Gies & Bolton 1982; Ninkov et al. 1987a, b; Brocksopp et al. 1999b), though there is some evidence to the contrary (Hutchings 1974, Bolton 1975, Hutchings 1978, Guinan et al. 1979). Therefore, Fourier components higher than second order in orbital frequency are generally ignored.

Orbital inclination i is related to the Fourier amplitudes in Equations 4.4a and 4.4b by

$$\left(\frac{1-\cos i}{1+\cos i}\right)^2 = \frac{(q_2+u_1)^2 + (q_1-u_2)^2}{(q_1+u_2)^2 + (q_2-u_1)^2} \tag{4.5a}$$

$$\left(\frac{1-\cos i}{1+\cos i}\right)^4 = \frac{(q_4+u_3)^2 + (q_3-u_4)^2}{(q_3+u_4)^2 + (q_4-u_3)^2} \tag{4.5b}$$

and the position angle of the line of quadratures (Dolan & Tapia 1989) is given by

$$\Theta_{\rm quad} = \frac{\Omega}{2} + 90^\circ \tag{4.6a}$$

$$\tan\Omega_a = \frac{D-T}{B-C} \tag{4.6b}$$

$$\tan\Omega_b = \frac{B+C}{D+T} \tag{4.6c}$$

$$B = \frac{u_4 - q_3}{(1-\cos i)^2} \tag{4.6d}$$

$$C = \frac{u_4 + q_3}{(1+\cos i)^2} \tag{4.6e}$$

$$D = \frac{q_4 - u_3}{(1+\cos i)^2} \tag{4.6f}$$

$$T = \frac{u_3 + q_4}{(1-\cos i)^2} \tag{4.6g}$$

according to Drissen et al. (1986a). Inclinations from Equations 4.5a and 4.5b, and values of Ω from Equations 4.6b and 4.6c, should be equal and provide a consistency check of the model. Because terms in i are raised to the even powers (Equations 4.5b and 4.5a), degeneracies exist between i and $i \pm 180^\circ$ as well as between Ω and $\Omega \pm 180^\circ$.

4.3.2 Inclination Bias

Inclination estimates from polarimetry are known to be biased toward high (edge-on) inclination, where the strength of the bias is inversely related to the signal to noise ratio of the data. For an edge-on geometry and a phase-locked, optically thin distribution of scatterers, symmetry dictates that the observed polarization will be either parallel or perpendicular to the orbital plane throughout the orbit. Therefore, the polarization components parallel and perpendicular to the orbital plane will be modulated sinusoidally, while the polarization components at $\pm 45^\circ$ with respect to the orbital plane will be zero during the orbit. Observed U versus Q will trace a line over the course of the orbit, where the position angle of that line in (Q, U) space will be related to the position angle of the line of quadratures in the plane of the sky.

Conversely, polarization observed from a face-on system will trace a circle in (Q, U) space due to symmetry. This is because a face-on system will have constant degree of polarization, $P(\lambda) = \sqrt{Q(\lambda)^2 + U(\lambda)^2}$, throughout the orbit. Since $P(\lambda)$ will be constant, $U(\lambda) = \pm\sqrt{P(\lambda)^2 - Q(\lambda)^2}$ is the equation of a circle in (Q, U) space. Given noisy data obtained on a system with arbitrary inclination, a linear fit to observed $U(\lambda)$ versus $Q(\lambda)$ will begin to have higher confidence. Consequently, low quality data will bias inverted inclination towards high values. For arbitrary inclination, truly phase-locked systems will trace out an ellipse in (Q, U) space, where BME and Rudy & Kemp (1978) independently discovered the eccentricity of the ellipse to be

$$e = \frac{\sin^2 i}{1 + \cos^2 i}. \tag{4.7}$$

Because of the polarimetric bias inherent to the BME technique, many authors (Milgrom 1978, Simmons et al. 1980, Aspin et al. 1981, Simmons et al. 1982, Wolinski & Dolan 1994) have criticized the use of formal error propagation when determining uncertainty in inclination. Uncertainty derived from error propagation, where inclination uncertainty is related to uncertainties in the Fourier

components of Equations 4.5a and 4.5b, dramatically overestimates the confidence in an inclination estimate. The standard mechanism for estimating the confidence interval on polarimetrically-derived inclination was developed by Aspin et al. (1981) and Simmons et al. (1982), and it was extended by Wolinski & Dolan (1994).

Consider a time series of $N = N_Q + N_U$ observations in Stokes Q and U wrapped to the binary's orbital phase. Let uncertainty in each observation be σ. The maximum and minimum values of the *fits* to $Q(\lambda)$ and $U(\lambda)$, as opposed to the maximum *observed* $Q(\lambda)$ and $U(\lambda)$, are denoted $q_{\max}$, $u_{\max}$, $q_{\min}$, and $u_{\min}$. The relevant quantity in determining data quality is the so-called "figure of merit" γ, which is effectively the square of the signal to noise ratio of each $Q(\lambda)$ and $U(\lambda)$ fit. The amplitude of polarimetric variability A and the figure of merit γ are given by

$$A = \frac{|q_{\max} - q_{\min}| + |u_{\max} - u_{\min}|}{4} \tag{4.8a}$$

$$\gamma = \left(\frac{A}{\sigma}\right)^2 \frac{N}{2} \tag{4.8b}$$

from Aspin et al. (1981) and Simmons et al. (1982), respectively.

Using the regularized Monte Carlo approach of Dolan (1984), Wolinski & Dolan (1994, hereafter WD94) generate $Q(\lambda, i)$ and $U(\lambda, i)$ curves expected from single scattering in a close binary. They calculate these curves for inclinations ranging from 0° to 90° in 5° increments. The primary is constructed from 5,000 elements that illuminate the scattering region. These authors take into account limb and gravity darkening of the primary as well as the change in projected area of the illuminating element as seen by the scatterer. WD94 add noise with zero mean and variance σ^2 to $Q(\lambda, i)$ and $U(\lambda, i)$, where 1,000 curves are generated for each inclination step. Based on the figures of merit of the synthesized data sets, they find confidence intervals on inclination derived from Equation 4.5b. WD94 recommend calculating i and γ from Equations 4.5b and 4.8b and determining the confidence interval on derived inclination from their Figure 4.

4.4 Results

For each night, the weighted mean polarization is taken for each Cassegrain ring angle, where the weight is proportional to number of detected photons. Uncertainty in each of these bins is the square root of the weighted variance of the measurements in the bin. These data are listed in Table 4.1, where $n_{\rm phot}$ is the number of detected photons, and $n_{\rm msmts}$ is the number of 30 second measurements, in each bin. Fitting Equations 4.4a and 4.4b to the binned data in Table 4.1, we obtain the Fourier coefficients listed in Table 4.2. Data from this work are listed as W07 and W08 for August 2007 and June 2008 obsevations, respectively. Kemp (1980b) data are denoted K80, and Dolan & Tapia (1989) data are DT89. These will be explained later.

The standard fit involves the zeroth, first, and second harmonics of the orbital frequency (listed in bold in Table 4.2). However, we have included additional fits, using only the zeroth and second harmonics as well as using the zeroth through third harmonics. The strength of the first harmonic is sensitive to the distribution of scatterers about the orbital plane, and the strength of the third harmonic is sensitive to orbital eccentricity. Binned data from August 2007 and June 2008 are plotted in Figures 4.1 and 4.2, respectively. The area of each open circle is proportional to the total number of detected photons in each bin.

The "max − min" values in Table 4.2 are the peak to peak differences in the fits for $Q(\lambda)$ and $U(\lambda)$. Fit χ^2, number of observations, and the significance level for fit rejection, α, are listed. The amplitudes of the first, second, and third harmonic components are given by

$$\begin{pmatrix} q_{\rm I} \\ q_{\rm II} \\ q_{\rm III} \end{pmatrix} = \begin{pmatrix} q_1^2 + q_2^2 \\ q_3^2 + q_4^2 \\ q_5^2 + q_6^2 \end{pmatrix}^{\frac{1}{2}} \tag{4.9a}$$

$$\begin{pmatrix} u_{\rm I} \\ u_{\rm II} \\ u_{\rm III} \end{pmatrix} = \begin{pmatrix} u_1^2 + u_2^2 \\ u_3^2 + u_4^2 \\ u_5^2 + u_6^2 \end{pmatrix}^{\frac{1}{2}} \tag{4.9b}$$

$$\begin{pmatrix} p_{\rm I} \\ p_{\rm II} \\ p_{\rm III} \end{pmatrix} = \begin{pmatrix} q_{\rm I}^2 + u_{\rm I}^2 \\ q_{\rm II}^2 + u_{\rm II}^2 \\ q_{\rm III}^2 + u_{\rm III}^2 \end{pmatrix}^{\frac{1}{2}} . \tag{4.9c}$$

Table 4.1: Journal of Observations

Data Set UT Date	MJD	Phase	Q (%)	U (%)	$n_{\rm phot}$ ($\times 10^7$)	$\theta_{\rm Cass}$ (°)	$n_{\rm msmts}$
W07	54314.477	0.5369	–	−4.355(42)	2.4	45	3
2007 Aug 2	54314.480	0.5375	0.632(49)	–	5.0	270	11
	54314.486	0.5385	–	−4.397(43)	5.2	225	12
	54314.487	0.5387	0.662(68)	–	5.0	180	12
	54314.501	0.5411	–	−4.474(61)	4.3	315	10
	54314.504	0.5418	–	−4.531(60)	4.1	135	11
	54314.511	0.5431	0.622(43)	–	3.8	0	9
2007 Aug 3	54315.332	0.6896	0.726(41)	–	4.5	90	4
	54315.344	0.6918	–	−4.658(45)	7.4	135	10
	54315.348	0.6924	–	−4.681(37)	16.1	45	52
	54315.349	0.6927	0.710(51)	–	16.8	0	56
	54315.351	0.6930	0.724(42)	–	8.0	180	12
	54315.357	0.6940	–	−4.684(22)	6.4	225	8
	54315.357	0.6941	0.698(31)	–	6.3	270	8
	54315.357	0.6941	–	−4.657(26)	6.3	315	8
2007 Aug 4	54316.325	0.8670	–	−4.821(22)	20.5	45	29
	54316.326	0.8672	0.589(61)	–	5.1	90	6
	54316.330	0.8678	–	−4.743(20)	4.5	135	4
	54316.336	0.8689	0.565(43)	–	23.0	0	36
	54316.341	0.8699	–	−4.776(31)	4.1	315	4
	54316.345	0.8705	0.578(50)	–	8.4	180	14
	54316.352	0.8717	–	−4.804(60)	6.6	225	10
	54316.352	0.8718	0.533(65)	–	6.0	270	8
2007 Aug 5	54317.300	0.0411	–	−4.597(23)	8.6	135	4
	54317.305	0.0419	0.482(67)	–	8.5	90	4
	54317.348	0.0497	0.504(43)	–	13.8	180	12
	54317.368	0.0532	–	−4.660(35)	23.6	45	36
	54317.368	0.0533	0.489(50)	–	23.7	0	36
	54317.375	0.0544	–	−4.649(31)	11.1	225	8
	54317.375	0.0544	–	−4.632(45)	11.0	315	8
	54317.375	0.0544	0.498(47)	–	10.8	270	8
2007 Aug 6	54318.351	0.2288	0.649(39)	–	17.7	180	12
	54318.352	0.2290	–	−4.773(23)	17.5	225	12
	54318.354	0.2293	0.640(38)	–	17.3	270	12
	54318.356	0.2296	–	−4.736(21)	17.3	315	12
	54318.373	0.2328	0.639(54)	–	28.2	0	32
	54318.377	0.2334	–	−4.782(23)	25.9	45	28
W08	54625.951	0.0698	–	−4.805(30)	7.8	135	6
2007 Jun 8	54625.958	0.0709	0.571(20)	–	7.7	90	6
	54625.976	0.0742	0.575(24)	–	11.5	0	14
	54625.977	0.0743	–	−4.819(14)	11.9	45	14
2007 Jun 9	54626.873	0.2344	0.759(20)	–	13.5	0	20
	54626.885	0.2366	–	−5.006(29)	13.7	45	20
	54626.897	0.2387	0.741(20)	–	14.3	90	20
	54626.909	0.2409	–	−4.982(20)	13.8	135	20
2007 Jun 10	54627.903	0.4182	0.522(25)	–	13.8	0	20
	54627.915	0.4204	–	−4.969(17)	13.7	45	20
	54627.927	0.4226	0.519(25)	–	14.5	90	20
	54627.939	0.4247	–	−4.958(18)	14.2	135	20
2007 Jun 11	54628.905	0.5973	0.617(24)	–	14.3	0	20
	54628.917	0.5994	–	−4.961(23)	14.3	45	20
	54628.929	0.6016	0.591(20)	–	14.8	90	20
	54628.941	0.6037	–	−4.947(29)	14.6	135	20
2007 Jun 12	54629.865	0.7687	0.643(20)	–	12.0	0	16
	54629.875	0.7705	–	−5.000(16)	12.2	45	16
	54629.885	0.7722	0.623(21)	–	12.4	90	16
	54629.895	0.7740	–	−4.985(18)	12.3	135	16
2007 Jun 13	54630.876	0.9491	0.541(28)	–	12.8	0	20
	54630.888	0.9513	–	−4.94(23)	12.9	45	20
	54630.900	0.9534	0.515(19)	–	13.0	90	20
	54630.912	0.9556	–	−4.902(21)	12.7	135	20
2007 Jun 14	54631.862	0.1252	–	−4.908(21)	13.4	135	20
	54631.874	0.1274	0.655(17)	–	13.5	90	20
	54631.886	0.1295	–	−4.913(24)	13.6	45	20
	54631.898	0.1317	0.675(27)	–	13.7	0	20

Table 4.2: BME Fit Parameters

Data Set	W08	W07			W_{mean}	K80	DT89	All
Fit Orders	**0,1,2**	0,2	**0,1,2**	0,1,2,3	0,1,2	0,1,2	0,1,2	0,1,2
Period (days)	**5.599829**	5.599829	**5.599829**	5.599829	5.599829	5.600	5.59974	5.599829
Epoch (MJD)	**51729.949**	51729.949	**51729.949**	51729.949	51729.949	41000.6	41868.610	51729.949
q_0 (%)	**+0.6044**	+0.5807	**+0.6102**	+0.6143	+0.6073	+0.6539	+1.1010	+0.7864
q_1 (%)	**+0.0051**	–	**−0.0734**	−0.0794	−0.0342	−0.0066	−0.0965	−0.0327
q_2 (%)	**+0.0312**	–	**−0.0225**	−0.0182	+0.0044	−0.0155	−0.0182	−0.0008
q_3 (%)	**−0.0894**	−0.0835	**−0.0612**	−0.0705	−0.0753	+0.0002	−0.0624	−0.0505
q_4 (%)	**+0.0378**	+0.0284	**+0.0152**	+0.0147	+0.0265	+0.0778	+0.1121	+0.0759
q_5 (%)	–	–	–	−0.0246	–	–	–	–
q_6 (%)	–	–	–	+0.0271	–	–	–	–
$q_{\rm I}$ (%)	**0.0316**	–	**0.0767**	0.0815	0.0344	0.0168	0.0982	0.0327
$q_{\rm II}$ (%)	**0.0971**	0.0882	**0.0631**	0.0720	0.0798	0.0778	0.1283	0.0912
$q_{\rm III}$ (%)	–	–	–	0.0366	–	–	–	–
$\frac{1}{2}(q_{\rm max} - q_{\rm min})$ (%)	**0.1140**	0.0882	**0.1187**	0.1491	0.0986	0.0890	0.2016	0.1119
χ^2_Q	**11.9**	25.4	**1.3**	1.3	–	–	–	–
n_Q	**14**	18	**18**	18	–	–	–	–
α_Q	**0.615**	0.115	**1.000**	1.000	–	–	–	–
u_0 (%)	**−4.9510**	−4.7052	**−4.6653**	−4.5972	−4.8082	−4.8603	−4.6000	−4.8038
u_1 (%)	**+0.0347**	–	**−0.1023**	−0.2095	−0.0338	+0.0075	−0.0572	−0.0050
u_2 (%)	**+0.0081**	–	**+0.0015**	+0.0837	+0.0048	+0.0165	+0.0789	+0.0345
u_3 (%)	**+0.0489**	+0.0728	**+0.1071**	+0.1292	+0.0780	+0.0594	+0.0722	+0.0602
u_4 (%)	**+0.0285**	+0.0908	**+0.0572**	−0.1047	+0.0429	+0.0335	+0.0792	+0.0471
u_5 (%)	–	–	–	+0.0795	–	–	–	–
u_6 (%)	–	–	–	+0.0526	–	–	–	–
$u_{\rm I}$ (%)	**0.0356**	–	**0.1023**	0.2256	0.0341	0.0181	0.0975	0.0349
$u_{\rm II}$ (%)	**0.0566**	0.1163	**0.1214**	0.1664	0.0890	0.0682	0.1072	0.0764
$u_{\rm III}$ (%)	–	–	–	0.0953	–	–	–	–
$\frac{1}{2}(u_{\rm max} - u_{\rm min})$ (%)	**0.0764**	0.1163	**0.1890**	0.3510	0.1120	0.0812	0.1702	0.1154
χ^2_U	**22.9**	86.6	**25.8**	23.6	–	–	–	–
n_U	**14**	19	**19**	19	–	–	–	–
α_U	**0.061**	1×10^{-10}	**0.135**	0.211	–	–	–	
$p_{\rm I}$ (%)	**0.0476**	–	**0.1279**	0.2399	0.0485	0.0247	0.1383	0.0478
$p_{\rm II}$ (%)	**0.1124**	0.1460	**0.1368**	0.1813	0.1196	0.1035	0.1672	0.1190
$p_{\rm III}$ (%)	–	–	–	0.1021	–	–	–	–
$p_{\rm I}/p_{\rm II}$	**0.42**	–	**0.93**	1.32	0.41	0.24	0.83	0.40
$\epsilon_{\rm I}$	**0.298**	–	**0.483**	0.458	0.289	0.193	0.453	0.287
$\epsilon_{\rm II}$	**0.702**	1	**0.517**	0.346	0.711	0.807	0.547	0.713
$\epsilon_{\rm III}$	–	–	–	0.195	–	–	–	–
A (%)	**0.0952**	0.1022	**0.1539**	0.2500	0.1053	0.0851	0.1859	0.1136
γ	**297**	163	**369**	974	666	–	287	–
$i_{\rm I}$, 1σ (°)	$\mathbf{49^{+6}_{-49}}$	–	**81 ± 1**	85 ± 1	89 ± 1	89	51^{+5}_{-51}	29
$i_{\rm I}$, 90% (°)	$\mathbf{49^{+8}_{-49}}$	–	**81 ± 2**	85 ± 2	89 ± 2	89	51^{+7}_{-51}	29
$i_{\rm I}$, 2σ (°)	$\mathbf{49^{+10}_{-49}}$	–	**81 ± 3**	85 ± 2	89 ± 2	89	51^{+9}_{-51}	29
$i_{\rm II}$, 1σ (°)	**78 ± 1**	68^{+4}_{-6}	**81 ± 1**	79 ± 1	76 ± 2	72	67^{+2}_{-4}	58
$i_{\rm II}$, 90% (°)	$\mathbf{78^{+2}_{-3}}$	68^{+5}_{-26}	**81 ± 2**	79 ± 2	76 ± 3	72	67^{+3}_{-13}	58
$i_{\rm II}$, 2σ (°)	$\mathbf{78^{+2}_{-4}}$	68^{+6}_{-45}	**81 ± 3**	79 ± 2	76 ± 3	72	67^{+4}_{-22}	58
Ω_a, 1σ (°)	**148 ± 3**	147 ± 8	**125 ± 3**	112 ± 3	136 ± 2	100	128 ± 8	126
Ω_a, 2σ (°)	**148 ± 7**	147 ± 16	**125 ± 6**	112 ± 7	136 ± 4	100	128 ± 14	126
Ω_b, 1σ (°)	**48 ± 3**	63 ± 8	**58 ± 3**	112 ± 3	51 ± 2	17	37 ± 8	35
Ω_b, 2σ (°)	**48 ± 7**	63 ± 16	**58 ± 6**	112 ± 7	51 ± 4	17	37 ± 14	35
$\Theta_{\rm quad,a}$, 1σ (°)	**164 ± 2**	164 ± 8	**153 ± 2**	146 ± 3	158 ± 2	140	154 ± 4	153
$\Theta_{\rm quad,a}$, 2σ (°)	**164 ± 4**	164 ± 16	**153 ± 3**	146 ± 7	158 ± 4	140	154 ± 7	153
$\Theta_{\rm quad,b}$, 1σ (°)	**114 ± 2**	121 ± 8	**119 ± 2**	146 ± 3	116 ± 2	98	109 ± 4	108
$\Theta_{\rm quad,b}$, 2σ (°)	**114 ± 4**	121 ± 16	**119 ± 3**	146 ± 7	116 ± 4	98	109 ± 7	108

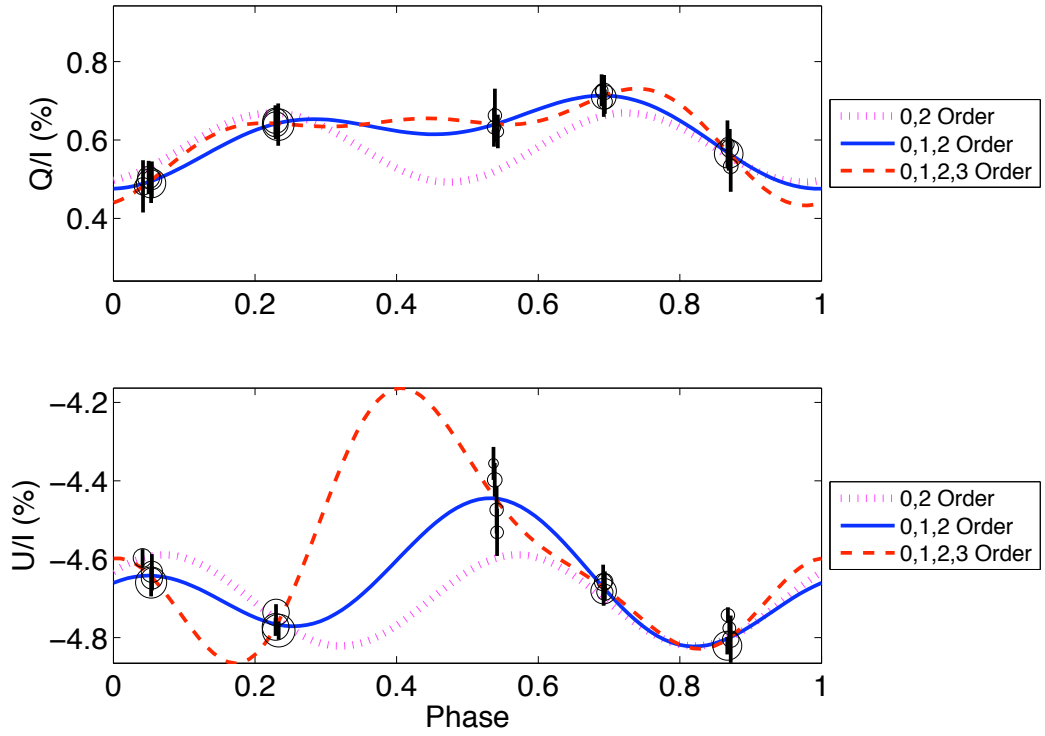

Figure 4.1: Binned observations of Cygnus X-1, August 2007 data. Area of each open circle is proportional to number of detected photons.

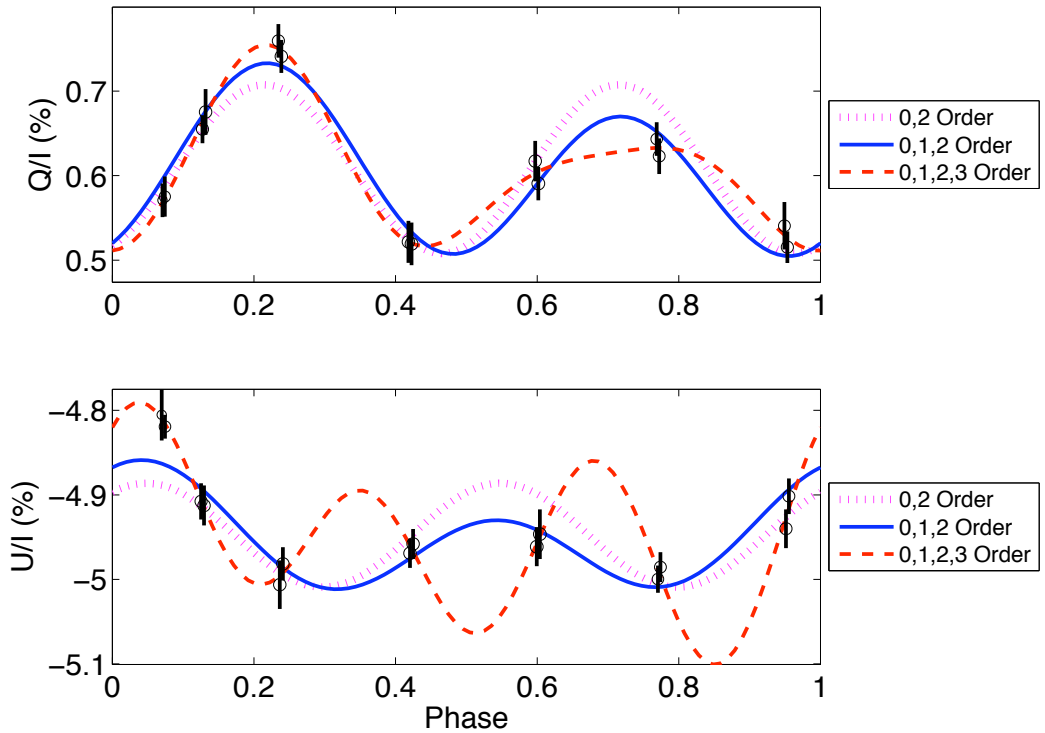

Figure 4.2: Binned observations of Cygnus X-1, June 2008 data. Observations at phase 0.13 correspond to the next orbit.

The fractional power in the first, second, and third harmonics for each fit are given as $\epsilon_{\rm I}$, $\epsilon_{\rm II}$, and $\epsilon_{\rm III}$, respectively, where $\epsilon_{\rm I} + \epsilon_{\rm II} + \epsilon_{\rm III} = 1$. We require that $\alpha > 0.01$ in order to assume the fit is valid. It should be noted that values higher than $\alpha = 0.01$ do not imply that the model is a correct physical description of the scattering process. Indeed, it is expected that the fits to the Aug 2007 data involving zeroth through second and zeroth through third order in orbital frequency will have favorable values of α, regardless of whether the model is actually correct. This is because these fits have five and seven parameters, respectively, while the data essentially consist of five points (one per night). The zeroth through third order fit to the Jun 2008 data is also expected to fit the data well, because seven nights of data were taken.

Values lower than $\alpha = 0.01$, however, imply that either (1) the model does not accurately describe high-frequency modulation in the data, or (2) the model does not correctly describe the scattering process. Since the scatter in observations during each night is low, we can assert that high-frequency fluctuations in the polarization from Cygnus X-1 are not observed. For the Aug 2007 run, the 0th/2nd harmonic model is the only one tested for which data overconstrain the fit, so α for this fit is the probability that the model accurately describes the physical processes involved. Thus, the discrepancy between the 0th/2nd harmonic model and both Stokes parameters observed at phase 0.55 is significant: the first harmonic is essential in describing the polarimetric modulation in Cygnus X-1 to a confidence level $1 - \alpha_Q \alpha_U \approx 1 - 10^{-11}$. The data from the Jun 2008 run overconstrain the zeroth through second order fit, which is the standard fit for the BME technique. The BME model can be rejected for this run at the $1 - \alpha_Q = 0.38$ and $1 - \alpha_U = 0.94$ confidence levels for the Stokes Q and U data, respectively. The inadequacy of the BME model is evidenced by the poor Stokes U fit seen in Figure 4.2.

The large contribution of the third harmonic is seen most strongly in the Stokes U data, and it is most likely spurious. Indeed, the fit using the zeroth through third harmonics is radically different between the Aug 2007 and Jun 2008 runs, which can be seen in Figures 4.1 and 4.2. A rapid increase in U occurs between observations near phase 0.4 during the Aug 2007 run, which is a strong indicator that it is an artifact of the fit. To test this, we generated random data sets consisting of five points each, where the phase of the data points correspond to the phases in Figure 4.1. While the Q and U value for each point was chosen randomly, mean Q and U as well as the amplitudes were set to the observed values. Each synthetic data set was fit to Equations 4.4a and 4.4b. An example of a random data set is given as Figure 4.3. The amplitudes $A_{\rm fit}$ and $A_{\rm data}$ are shown as dashed and dotted lines, respectively.

Both a histogram of the ratio of amplitudes $A_{\rm fit}/A_{\rm data}$ and their cumulative distribution function (CDF) are plotted in Figure 4.4 for the randomly generated data sets. Ratios must be larger than unity, because the five-parameter fit will always pass through each five-point data set. Large ratios of amplitudes indicate that the fits have large fluctuations for phases between data points. For the 0th/1st/2nd order fit to the observations in Figure 4.1, the measured values of $A_{\rm fit}/A_{\rm data}$ are 1.08 and 1.10 for Q and U, respectively. The probabilities of random data having higher amplitude ratios are $1 - {\rm CDF}_Q = 88\%$ and $1 - {\rm CDF}_U = 87\%$, indicating the high probability that the 0th/1st/2nd order fit accurately represents the polarization during phases in which the system was not observed. However, $A_{\rm fit}/A_{\rm data}$ increases to 1.36 and 2.03 for the fit including the third harmonic. These ratios are lower than 43% and 5% of random data. Thus, the fits including the third harmonic have low probability of accurately describing the system, especially for the U fit. Since the third harmonic is generated by orbital eccentricity, the fact that the third harmonic is not necessary to fit the observed data agrees with the observation that orbital eccentricity is consistent with zero. Thus, we agree with the community's use of the 0th/1st/2nd order fit as being the most appropriate for Cygnus X-1.

For the Aug 2007 data, inclination determined from the first-order coefficients in Equation 4.5a is $i_{\rm I} = 81.2^\circ$, while the second-order coefficients give $i_{\rm II} = 81.3^\circ$ from Equation 4.5b. Thus, inclinations derived from the first and second order coefficients are mutually consistent. However, inclinations derived from the Jun 2008 data are $i_{\rm I} = 48.9^\circ$ and $i_{\rm II} = 77.8^\circ$, which are mutually inconsistent. To estimate the confidence interval on these inclinations, we first determine the figure of merit γ (Equation 4.8b). Since each bin has a different uncertainty, we choose to rewrite Equation 4.8b as a summation over bins j:

$$\gamma = \frac{1}{2} \sum_{j=1}^{N} \left(\frac{A}{\sigma_j} \right)^2 . \tag{4.10}$$

To estimate the confidence interval on our derived inclination estimate, we consult Figure 4 of WD94 for $\gamma = 300$, which is plotted in Figure 4.5. Interpolating between the confidence intervals for $\gamma = 300$ and $\gamma = 1.2 \times 10^5$ in the same figure shows that the difference between $\gamma = 300$ and $\gamma = 369$ reduces the confidence interval by less than one degree. Therefore, we estimate the confidence intervals on derived inclination to be $80^\circ \leq i \leq 82^\circ$ (1σ) and $78^\circ \leq i \leq 84^\circ$ (2σ) for the Aug 2007 data. The 90% confidence interval is therefore $79^\circ < i < 83^\circ$. For the Jun 2008 run, the confidence intervals on derived inclination are $77^\circ \leq i \leq 79^\circ$ (1σ), $75^\circ \leq i \leq 80^\circ$ (90% confidence), and $74^\circ \leq i \leq 80^\circ$

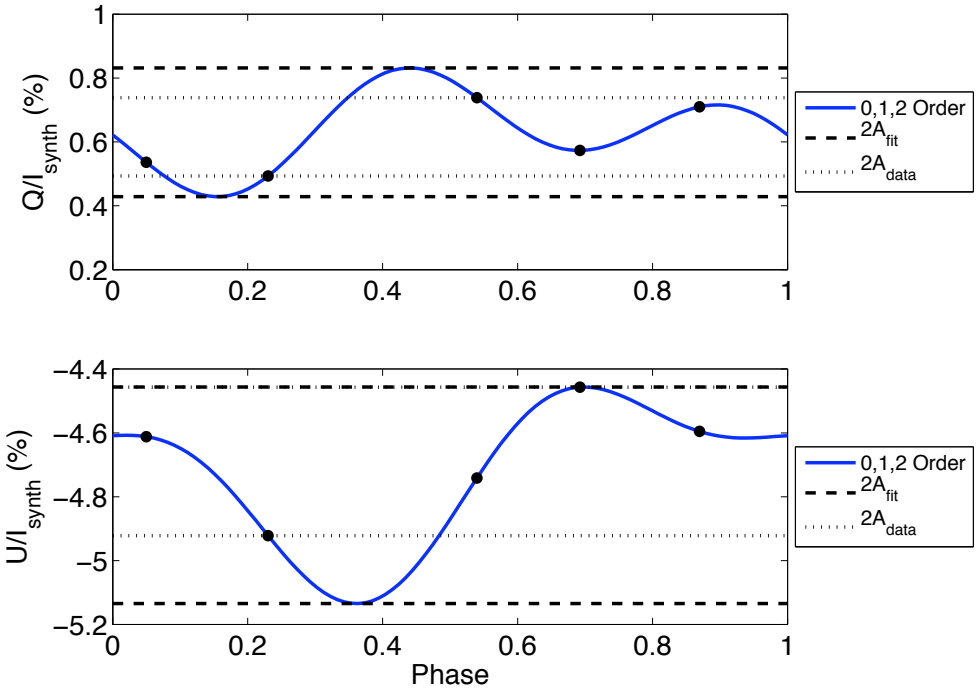

Figure 4.3: Examples of synthesized Q and U data sets. Extrema lying at phases between data points suggest that the fits do not accurately describe the system at all phases.

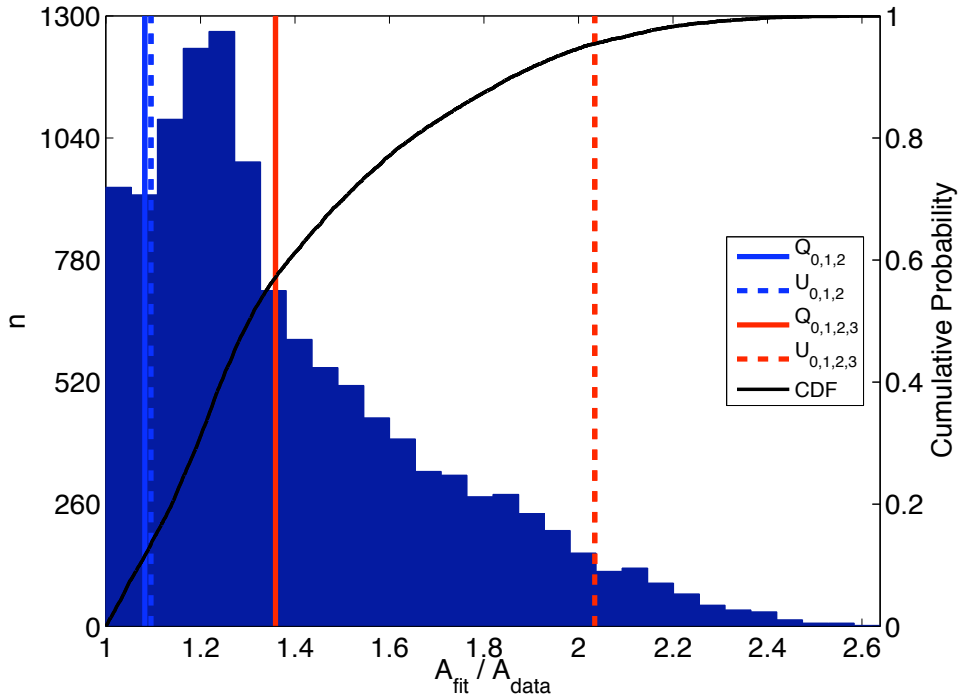

Figure 4.4: Histogram (left axis) and cumulative distribution function (right axis) of the ratios of amplitudes between BME fits and synthesized data. Large ratios indicate that the fit surpasses the range of the data.

(2σ). We find the values of $\Theta_{\rm quad}$ from Equations 4.6b and 4.6c to be inconsistent for both the Aug 2007 and Jun 2008 runs.

4.5 Literature Estimates

Other groups have estimated the inclination of Cygnus X-1 as well as other binary systems (Table 4.3 and Figure 4.6). Uncertainties in parenthesis represent 1σ error, while ranges indicate 90% confidence intervals. An inclination of "?" indicates that the inclination inversion method failed to provide a fit at acceptable significance under the χ^2 test. Methods used generally fall into four categories: presence/lack of eclipses, radial velocity (mass function or tomography), ellipsoidal light modulation, and polarimetry.

4.5.1 Eclipses

Strong X-ray eclipses are not observed in Cygnus X-1, so the maximum allowable inclination is given by $\cos i_{\rm max} = R/a$, where R is the radius of the supergiant and a is the semimajor axis of the orbit (Figure 4.7). These values are estimated at $a = 40.2\ R_\odot$, $42 \pm 9\ R_\odot$ (Herrero et al. 1995, Iorio 2007), $R = 18\ R_\odot$, 17.0 to 22.9 $R_\odot$, $22.77 \pm 2.3\ R_\odot$ (Bochkarev et al. 1975, Herrero et al. 1995, Ziólkowski 2005), and $R/a = 0.4$ to 0.45 (Karitskaya & Bochkarev 1989). Thus, the maximum inclination is $i_{\rm max} \approx 62 \pm 4^\circ$. This is inconsistent with the inclinations derived from individual runs at the $4\sigma - 5\sigma$ level. Thus, we can state with high confidence that the BME technique fails when determining the inclination of Cygnus X-1 from single-orbit observing runs. The maximum inclination is inconsistent at the 3σ level with the polarimetric modulation when co-adding both runs.

4.5.2 Radial Velocity Mass Function

Estimation of inclination from the radial velocity mass function proceeds from *a priori* knowledge of the masses of both binary components, which is usually estimated by stellar evolution modeling from observed spectral type (cf. Moffat et al. 1990a). Inclination is then derived from the definition of the mass function:

$$f(M_{\rm BH}) = \frac{M_{\rm BH} \sin^3 i}{\left(1 + M_{\rm star}/M_{\rm BH}\right)^2}. \tag{4.11}$$

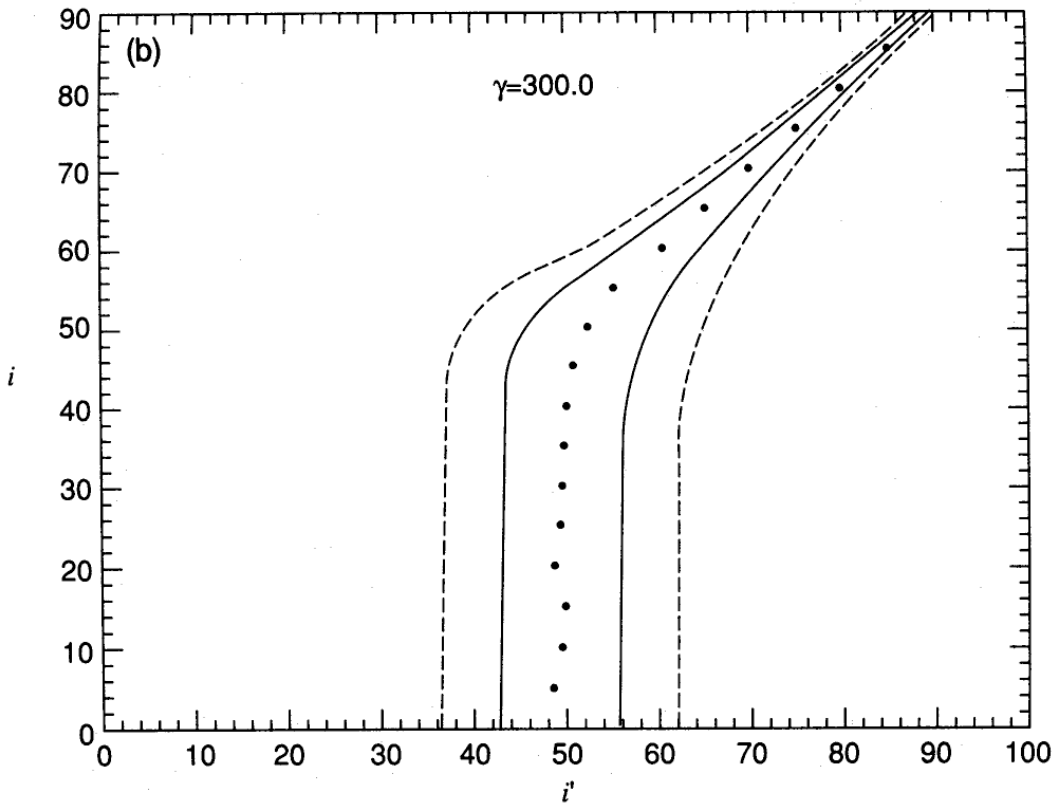

Figure 4.5: Confidence intervals for inclination estimates from the BME model, taken from Figure 4 of Wolinski & Dolan (1994). Derived inclination is i' and true inclination is i. The solid lines indicate the 1σ confidence interval, while the 2σ confidence interval is given by dashed lines. Therefore, derived inclination $i' \leq 56°$ will have a 1σ confidence interval that extends down to $i = 0°$.

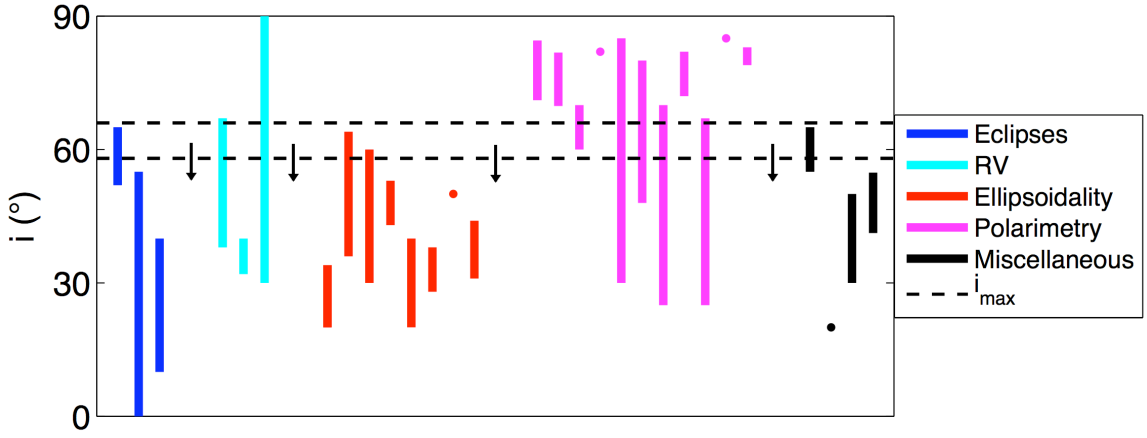

Figure 4.6: Cygnus X-1 inclination estimates from various methods. Note that many inclination estimates derived polarimetrically significantly exceed the maximum possible inclination, which is determined from the lack of observed X-ray eclipses.

Table 4.3: Comparison of Inclination Estimates

Binary	Reference	Method or Data	Band	i (°)
Cygnus X-1[1]	Bochkarev et al. (1979)	Minor eclipses	–	58(7)
	Sowers et al. (1998)	Wind non-eclipses	Hα	< 55
	Wen et al. (1999)	Minor eclipses	X-rays	25(15)
	This work	Non-eclipses	X-rays	$< 62 \pm 4$
	Karitskaya & Bochkarev (1989)	Disk precession	V	60(5)
	Brocksopp et al. (1999a)	···	X-rays	20
	Miller et al. (2002)	Disk spectrum	X-rays	40(10)
	Shaposhnikov & Titarchuk (2007)	QPO scaling	–	8.7(8) $M_\odot$
	Iorio (2007)	S&T (2007)	–	48.0(6.8)
	Ninkov et al. (1987a)	Mass function	–	36(4)
	Davis & Hartmann (1983)	RV tomography	U	52(15)
	Gies et al. (2003)	···	Hα	$> 30(7)$
	Hutchings et al. (1973)	Ellipsoidality	B	27(7)
	Bochkarev et al. (1975)	···	–	50(14)
	Hutchings (1978)	···	–	45(15)
	Guinan et al. (1979)	···	–	48(5)
	Brocksopp et al. (1999b)	···	UBV	50
	Gies & Bolton (1986a)	Ellip. + RV	–	33.5(5.5)
	Abubekerov et al. (2004)	···	–	37.5(6.5)
	Daniel (1981)	Ellip. + polarimetry	–	30(10)
	Kemp et al. (1978a)	Polarimetry	V	77.8(6.7)
	···	···	UV	75.8(6.0)
	Kemp et al. (1979)	···	–	65(5)
	Kemp (1980b)	···	–	82
	Simmons et al. (1980)	Kemp et al. (1979)	–	$30 - 85$
	···	Kemp (1980b)	–	$48 - 80$
	Long et al. (1980)	Polarimetry	X-rays	$25 - 70$
	Drissen et al. (1986a)	Kemp et al. (1978a)	–	77(5)
	Dolan & Tapia (1989)	Polarimetry	B	67
	···	···	V	55
	···	···	R	60
	···	···	BVR	$25 - 67$
	Wolinski et al. (1996)	···	U	85
	This work (W07)	···	$\approx B$	$79 - 83$
	··· (W08)	···	$\approx B$	$75 - 80$
	··· (W_{mean})	···	$\approx B$	$73 - 79$
Vela X-1[1,2]	Hutchings (1974)	Eclipses	–	80
(GP Vel)	Hutchings (1978)	···	–	73
(HD 77581)	Dolan & Tapia (1988)	Polarimetry	–	$67 - 81$
(4U 0900 − 40)	Wolinski et al. (1996)	···	U	?
HD 153919[1,2]	Hutchings (1974)	Eclipses	–	90
(V884 Sco)	Hutchings (1978)	···	–	87(3)
(4U 1700-37)	Dolan & Tapia (1984)	Polarimetry	–	85(3)
	Dolan & Tapia (1988)	···	U	53
	···	···	B	80
	···	···	R	84
	···	···	I	85
	···	···	$UBRI$	$71 - 86$
	Wolinski et al. (1996)	···	U	85
HD 152667	Dolan & Tapia (1988)	Polarimetry	U	83
(V861 Sco)	···	···	B	80
	···	···	G	85
	···	···	R	84
	···	···	I	86
	···	···	$UBGRI$	$75 - 90$
CX Dra	Horn et al. (1992)	Polarimetry	U	71
	Berdyugin & Piirola (2002)	Polarimetry	U	71
	···	···	U	75
	···	···	B	72
	···	···	B	70
	···	···	V	72
	···	···	V	66
	···	···	R	76
	···	···	R	81
	···	···	I	74
	···	···	I	86
	···	···	$UBVRI$	$65 - 76$ (2σ)
	···	···	$UBVRI$	$58 - 80$ (2σ)
Algol[2]	Batten (1967)	Eclipses	–	82
(β Per)	Rudy & Kemp (1978)	Polarimetry	–	81(4)
(HD 19356)	Aspin & Simmons (1982)	R&K (1978)	–	?

[1]High mass X-ray binary
[2]Eclipsing binary

Comparison of Inclination Estimates (continued)

Binary	Reference	Method or Data	Band	i (°)
W Ser[2]	Piirola et al. (2005)	Polarimetry	U	69.6
	···	···	U	64.3
	···	···	B	70.3
	···	···	B	56.3
	···	···	B	73.7
	···	···	V	78.3
	···	···	V	67.5
	···	···	R	74.1
	···	···	R	50.0
	···	···	I	79.0
	···	···	I	51.0
	···	Kruszewski (1972)	B	88.2
	···	···	G	82.7
AO Cas[2]	Batten (1967)	Eclipses	–	57
(HD 1337)	Rudy & Kemp (1978)	Polarimetry	–	63(9)
(HR 65)	Aspin & Simmons (1982)	R&K (1978)	–	0 − 88
σ Ori E[2]	Kemp & Herman (1977)	Polarimetry	B	76(8)
(HD 37479)	Aspin & Simmons (1982)	K&H (1977)	B	?
u Her[2]	Merril (1963)	Eclipses	–	77
(HD 156633)	Batten (1967)	···	–	76
(68 Her)	Rudy & Kemp (1978)	Polarimetry	–	77(5)
(HR 6431)	Aspin & Simmons (1982)	R&K (1978)	–	0 − 90
U Sge[2]	Batten (1967)	Eclipses	–	90
(HD 181182)	Rudy & Kemp (1978)	Polarimetry	–	87(3)
(HR 7326)	Aspin & Simmons (1982)	R&K (1978)	–	0 − 90
MWC 1080[2]	Manset & Bastien (2001)	Polarimetry	–	43 − 81
HD 47129	Rudy & Herman (1978)	Polarimetry	B	71(9)
(Plaskett's Star)	Aspin & Simmons (1982)	R&H (1978)	–	0 − 90
NTTS 162814 − 2427	Jensen & Mathieu (1997)	Mass function	–	71
	Manset & Bastien (2003)	Polarimetry	–	86.2(2.6)
WR 6 (EZ CMa)[3]	McLean (1980)	Polarimetry	–	71.4(6.8)
WR 9[2,3]	Lamontagne et al. (1996)	Eclipses	–	56.8(2.0)
(V443 Pup)	Niemela et al. (1984)	Mass function	–	64
(HD 63099)	···	Polarimetry	–	67.9(3.0)
WR 21[2,3]	Balona et al. (1989)	Eclipses	–	49.6(3.7)
(HD 90657)	Massey (1981)	Mass function	–	45
	Niemela (1982)	···	–	48
	Lamontagne et al. (1996)	Polarimetry	–	62.4(2.2)
WR 31[2,3]	Lamontagne & Moffat (1987)	Eclipses	–	61.6(1.7)
(V428 Car)	Niemela et al. (1985)	Mass function	–	40
(HD 94546)	Lamontagne et al. (1996)	Polarimetry	–	62.0(2.7)
WR 42[2,3]	Balona et al. (1989)	Eclipses	–	40.3(2.9)
(V431 Car)	Massey (1981)	Mass function	–	35
(HD 97152)	Davis et al. (1981)	···	–	38
	St.-Louis et al. (1987)	Polarimetry	–	39 − 49
CD Cru[2,3]	Moffat et al. (1990b)	Eclipses	–	63(7)
(WR 47)	Massey (1981)	Mass function	–	70
(HD 311884)	Moffat et al. (1990b)	···	–	90
	Moffat & Seggewiss (1987)	Polarimetry	–	77
	St.-Louis et al. (1988)	···	–	76.9(1.7)
	Moffat et al. (1990b)	···	–	73(5)
WR 79[2,3]	St.-Louis et al. (1987)	Eclipses	–	33.6(2.3)
(HD 152270)	Massey (1981)	Mass function	–	25
(HR 6265)	Seggewiss (1974)	···	–	34
	Luna (1982)	Polarimetry	–	42(10)
	St.-Louis et al. (1987)	···	–	40 − 50
WR 97[2,3]	Lamontagne et al. (1996)	Eclipses	–	?
(HD 320102)	Niemela (1995)	Mass function	–	31
	Lamontagne et al. (1996)	Polarimetry	–	85.4(2.0)
CV Ser[2,3]	Massey (1981)	Mass function	–	70
(WR 113)	Massey & Niemela (1981)	···	–	90
(HD 168206)	Lipunova (1982)	Eclipses	–	70.4(2.3)
	Lamontagne et al. (1996)	Polarimetry	–	79.7(2.3)
QY Vul[2,3]	Moffat & Shara (1986)	Eclipses	–	55.3(4.7)
(WR 127)	Massey (1981)	Mass function	–	70
(HD 186943)	Massey et al. (1981)	···	–	90
	St.-Louis et al. (1988)	Polarimetry	–	0 − 90
V444 Cyg[2,3]	Kron & Gordon (1950)	Eclipses	–	78.4
(WR 139)	Batten (1967)	···	–	80
(HD 193576)	Cherepashchuk (1975)	···	–	78(1)
	Hiltner & Mook (1966)	Polarimetry	–	76(6)
	Rudy & Kemp (1978)	···	–	72(6)
	Aspin & Simmons (1982)	R&K (1978)	–	0 − 90
	Piirola & Linnaluoto (1988)	Polarimetry	–	82.8(0.9)
	Robert et al. (1990)	H&M (1966)	–	83.2(4.3)
	···	R&K (1978)	–	76.0(2.3)
	···	Polarimetry	–	77 − 79
WR 148[3]	Drissen et al. (1986a)	Polarimetry	–	66.6(4.0)
CX Cep[2,3]	Massey & Conti (1981a)	Eclipses	–	≥ 50
(WR 151)	Lipunova & Cherepashchuk (1982)	···	–	50

[3]Wolf-Rayet binary

Comparison of Inclination Estimates (continued)

Binary	Reference	Method or Data	Band	i (°)
	De Greve et al. (1988)	···	–	51
	Schulte-Ladbeck & van der Hucht (1989)	Polarimetry	–	74(5)
	Villar-Sbaffi et al. (2006)	S-L&vdH (1989)	–	68(18)
	···	Kartasheva (2002b)	–	79(12)
	···	Polarimetry	–	70(2)
	···	···	U	89^{+1}_{-7}
	···	···	B	76(14)
	···	···	V	86^{+4}_{-9}
	···	···	R	81(8)
	···	···	I	87^{+3}_{-8}
GP Cep[2,3]	Moffat & Shara (1986)	Eclipses	–	74.0(0.7)
(WR 153)	St.-Louis et al. (1988)	Polarimetry	–	78(5)
CQ Cep[2,3]	Leung et al. (1983)	Eclipses	–	68.0(0.4)
(WR 155)	Stickland et al. (1984)	···	–	70(4)
(HD 214419)	Drissen et al. (1986b)	Polarimetry	–	78.0(1.0)
	Piirola & Linnaluoto (1988)	···	–	78.1(1.7)

Here, $M_{\rm BH}$ is the mass of the black hole and $M_{\rm star}$ is the mass of the visible binary component. Modeling of the mass of the optical component is highly error-prone because of uncertainties both in the distance to the system and in evolutionary modeling. Therefore, inclination determined from the radial velocity mass function should only serve as a rough guide when no other inclination estimates exist.

4.5.3 Radial Velocity Tomography

Radial velocity tomography is used on stars exhibiting P Cygni profiles, and therefore on stars exhibiting mass loss. It is generally assumed that outflow velocity from all stellar latitudes is isotropic, so the radial velocity of the blueshifted absorption should be equal in magnitude, but opposite in sign, to the radial velocity of the redshifted emission for a nearly edge-on orientation at phase 0.5 (a truly edge-on geometry would exhibit no redshifted emission due to occultation by the supergiant). At this phase, the black hole is in superior conjunction, so the radial velocity of the supergiant is zero in a frame comoving with the system center of mass.

For stars nearly filling their Roche lobes, the density enhancement in the focused stellar wind will cause most of the redshifted P Cygni emission to be from material in the plane of the orbit. Thus, emission radial velocity will be related to absorption radial velocity by $v_{\rm em} = v_{\rm abs} \sin i$ (Figure 4.7). G03 acknowledge that the assumption of isotropic wind velocity is most likely not correct. Friend & Castor (1982) suggest that the enhanced density in the plane of the orbit, due to the focused stellar wind, will slow the equatorial wind with respect to the wind flowing toward the observer. Since decreased wind velocity in the plane of the orbit will bias the derived inclination towards lower values, inclinations determined by radial velocity tomography represent lower limits.

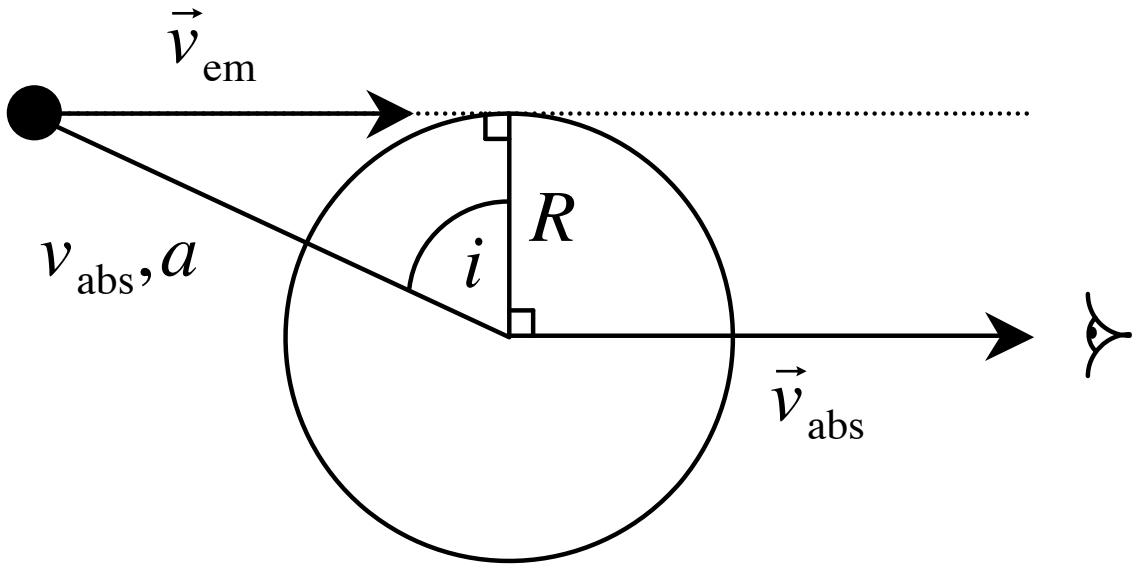

Figure 4.7: Geometry for eclipses and for radial velocity tomography. Arrows indicate P Cygni emission towards the observer. The magnitude of the absorption radial velocity $v_{\rm abs}$ has been scaled to the semimajor axis a; however, the semimajor axis and supergiant radius R are not to scale.

4.5.4 Ellipsoidal Modulation

The cross-sectional area of the tidally distorted supergiant varies at twice the orbital frequency, generating a so-called "ellipsoidal" lightcurve. In analogy to the modulation of polarization degree throughout the orbit, the lightcurve is indicative of orbital inclination. However, this technique assumes that the only photometric variability in the system is due to the ellipsoidality of the star. The focused stellar wind contributes to the flux from the system, which complicates ellipsoidal fitting. Cygnus X-1 is known to have an inclined, precessing accretion disk (section 4.2.2), so flux reflected off the disk generates a periodic phase shift with ≈ 150 and/or 294 day period added to the total system flux. Therefore, inclination of Cygnus X-1 derived from ellipsoidal modulation may not be equal to the physical inclination of the system.

When flux from the visible binary component dominates the system lightcurve, however, inclinations inverted from the ellipsoidal modulation technique can be very precise. For example, the X-ray luminosity of the black hole binary GRO J1655 − 40 is low during quiescence; therefore, accretion is low during this state. The visible, F5IV component dominates the optical and near-IR flux from the system, so ellipsoidal lightcurve fitting can yield accurate inclination. Greene et al. (2001) find $i_{\rm J1655} = 70.2 \pm 1.9$ (2σ) from $BVIJK$ band photometry and a black hole mass of $M_{\rm J1655} = 6.3 \pm 0.5$ $M_{\odot}$.

4.5.5 Polarimetry

The first Cygnus X-1 inclination estimate via polarimetry came from Kemp et al. (1978a, hereafter K78). From 180 nights of data taken over two years on a 61 cm telescope, they find strong second harmonic modulation in V band and weak modulation in U band. K78 phase-wrap the data onto an ephemeris generated by their own photometric data, and they bin the data at certain phase intervals to account for random fluctuations from orbit to orbit. K78 observe an ellipse in the (Q, U) plane, and they determine an inclination of $i = 77.8 \pm 6.7^\circ$ by fitting for the eccentricity of this ellipse (Equation 4.7). Uncertainty in inclination was calculated by formal error propagation from uncertainties in the amplitudes of the first and second Fourier harmonics (Equations 4.4a and 4.4b).

Kemp et al. (1979, hereafter K79) phase-wrap and bin 348 nights of data, including the data from K78. After smoothing third and higher harmonics, they show a (Q, U) locus that has significant departures from ellipticity. They state that this cannot be reconciled with the symmetric, canonical model of BME, which assumes symmetry in scatterers above and below the orbital plane. To explain their observed polarization, K79 suggest a model involving eclipses of a hot spot generated at the intersection of the supergiant's gas stream and the accretion disk. The model requires the hot spot to be eclipsed by a geometrically thick accretion disk when the black hole is at inferior conjunction (phase 0.5), which implies an inclination of $i = 65 \pm 5^\circ$. Milgrom (1978) and Kemp (1980a) propose that the accretion disk is flared due to irradiation by the X-ray source, and Kemp (1980a) model the inclination to be $i = 67.5 \pm 2.5^\circ$.

Simmons et al. (1980, hereafter S80) object to the dismissal by K79 of the applicability of the BME canonical model to Cygnus X-1, and they use both the symmetric and asymmetric canonical models to fit the data of K79. The asymmetric model allows the distribution of scatterers to be asymmetric about the orbital plane, which generates first harmonic periodicity in the polarization curves. S80 also criticize the small inclination uncertainties of K78 and K79 on the grounds that fits with a larger range of inclinations could acceptably represent the data in a χ^2 analysis. They argue that the 90% confidence interval on inclination from K79 should in fact be $i = 78^{+7^\circ}_{-48^\circ}$. The asymmetry in error bounds comes from the fact that a given increase in inclination causes a stronger change in the polarimetric signal than does a decrease in inclination by the same amount. In addition, S80 criticize the massive phase-binning of the K78 data to form mean polarization curves, because orbit-to-orbit changes of unknown cause are observed. S80 recommend observations with

larger telescopes to minimize uncertainty on each data point. This allows inclination inversion across data obtained over fewer orbits.

In the same volume as S80, Kemp (1980b, hereafter K80) reject the asymmetric canonical model of BME as an accurate representation of their phase-binned data, which now consist of 528 nights. While the asymmetric BME model predicts only first, second, and third harmonic modulation of polarization in a binary, K80 observe weak first harmonic and strong second through fifth harmonic modulations. They claim a probabillity of only 60% that the first harmonic is even present in their data, while the probability of the third through fifth being present is 85% as a group. Further, they observe the fifth harmonic at a significance of 99%.

K80 suggest that the physical reasoning for first harmonic modulation in the BME model, asymmetry in scatterers about the orbital plane, should also generate harmonics higher than the second. They state that any model that incorporates the first harmonic should be accepting of third and higher harmonics as well. Thus, they assume the only model of BME with any validity is the symmetric canonical model, which only assumes second harmonic modulation. K80 fit their data to the symmetric model to find an inclination of $i = 82°$. Unfortunately, no uncertainty is provided on this inclination estimate, and K80 do not address the issue of underestimation of inclination uncertainty raised by S80.

K80 assume that orbit-to-orbit variations in polarization are random, because uncertainty in phase bins is observed to decrease as the inverse square root of the number of observations. K80 claim that their large, phase-binned data set is therefore a true representation of the mean state of Cygnus X-1. Since a true inclination of $i = 82°$ would cause X-ray eclipses, K80 reconcile their inclination estimate with the lack of observed X-ray eclipses by claiming that shadowing or variable absorption are driving the polarimetrically-derived inclination toward higher values. Thus, K80 claim that the inclination of Cygnus X-1 is large but less than $i = 82°$. Finally, K80 disagree that larger telescopes and shorter observing epochs are the best way to minimize observational uncertainty, because they claim the "intrinsic noise" of Cygnus X-1 can have timescales longer than one month.

In proof, S80 caution that the addition of higher harmonics in data fitting will always generate a better fit; however, a better fit does not necessarily imply a more accurate representation of the

physical processes involved. S80 find the asymmetric canonical model acceptably fits the data of K80 at 10% significance, and the 90% confidence interval on derived inclination is $i = 71^{+9^\circ}_{-23^\circ}$. They find the symmetric canonical model implies $i = 70 \pm 8^\circ$ with a fit acceptable at only 5% significance. S80 admit that the unknown cause of the orbit-to-orbit polarimetric variations in Cygnus X-1, and therefore the unknown statistical distribution of those variations, makes an optimum observing campaign difficult to plan. Thus, S80 suggest that a short observing run on a large telescope be performed to test the validity of massive phase-binning of data.

Long et al. (1980) observe significant polarization of Cygnus X-1 in X-rays which they attribute to scattering of the X-ray source off the accretion disk. For an optically thick disk, polarization is expected to be parallel to the major axis of the disk when projected onto the plane of the sky (Angel 1969, Sunyaev & Titarchuk 1985, Phillips & Mészáros 1986, Kartje & Königl 1991), which implies a disk inclination of $i_{\rm disk} = 59.5 \pm 10.5^\circ$ (1σ). However, an optically thin disk is expected to be polarized perpendicular to the major axis (Shakhovskoi 1965, Pringle & Rees 1972, Shakura & Syunyaev 1973), which suggests $i_{\rm disk} = 35 \pm 10^\circ$ (1σ). The disk is thought to be optically thick with $\tau \approx 1 - 2$ (Syunyaev & Trümper 1979; Zdziarski et al. 1996, 1997; Gierliński et al. 1997; Poutanen 1998; Di Salvo et al. 2001; Frontera et al. 2001; Miller et al. 2002; Zdziarski & Gierliński 2004; Ibragimov et al. 2005; Ibragimov et al. 2007), so the inclination estimate of $i_{\rm disk} = 59.5 \pm 10.5^\circ$ (1σ) seems more likely. Since the disk is thought to be inclined, $i - \delta \leq i_{\rm disk} \leq i + \delta$ depending on disk precession phase. Here, δ is disk obliquity, which is estimated to be $\delta = 15 \pm 7^\circ$ (Karitskaya & Bochkarev 1989, Ibragimov et al. 2007). Therefore, orbital inclination is $i_{\rm disk} - \delta \leq i \leq i_{\rm disk} + \delta$, which implies $i = 60 \pm 13^\circ$.

Daniel (1981, hereafter D81) criticize the interpretation of K79 of eclipsing of a scattering region at the rim of the accretion disk on its *ad hoc* nature. Since tidal distortion of the supergiant causes the ellipsoidal lightcurve, and that Daniel (1980) suggest prolate ellipsoids can be up to 5% polarized, D81 assume the variability in polarization of the system is dominated by the tidal distortion of the supergiant, which is modeled to be ellipsoidal in shape. By simultaneously fitting the lightcurve and the modulation of polarization degree from the data of K79, D81 arrive at an inclination of $i = 30 \pm 10^\circ$. However, D81 acknowledge that modeling the polarization degree, instead of Stokes Q and U separately, introduces additional uncertainty to their inclination estimate.

While Bochkarev et al. (1979) caution against the approximation of the shape of the photosphere by an ellipsoid, they support the hypothesis that the tidally distorted supergiant causes the polari-

metric variability of the system. These authors model the amplitude of polarimetric variability of Cygnus X-1 to be $\Delta P_{\rm star} = 0.3\%$ from pure Thomson scattering by the Roche lobe-filling supergiant. However, Bochkarëv et al. (1986) model the distribution of the single-scattering albedo as well as scatterers in the Roche lobe-filling photosphere and find the variability amplitude to be only $\Delta P_{\rm star} = 0.023\%$, which is a full order of magnitude weaker than the observed variability (Table 4.2).

Dolan & Tapia (1984, 1988) observe changes in polarization curves on a ≈ 10 day timescale in HD 152667, HD 153919, and Vela X-1, which are also close binaries with OB supergiant primaries. Dolan & Tapia (1992, hereafter DT92) note that polarization curves of Cygnus X-1 taken 10 months apart on a 1.5m telescope are inconsistent at the $< 10^{-5}$ level of significance. Dolan & Tapia (1989, hereafter DT89) and DT92 therefore object to phase-binning, obtained over many orbital cycles, by K78, K79, and K80. DT89 and DT92 subscribe to the view of S80 that inclinations derived from single-orbit observations are more accurate in estimating the true orbital inclination of these binaries. Using the asymmetric canonical model of BME, as well as the method of S80, Aspin et al. (1981), and Simmons et al. (1982) for estimation of inclination uncertainty, DT89 determine the inclination of Cygnus X-1 to be $i = 62^{+5^\circ}_{-37^\circ}$ (90% confidence interval). This range is so large that it not only offers no additional constraint on the inclination of the system, but it also provides no confirmation of previous constraints.

DT89 and DT92 note that tidal distortion polarization (TDP) biases inclinations derived from the BME model toward higher values. In addition, it is not possible to subtract this component from the observed polarization curves before fitting to the BME model, because TDP is inclination-dependent. However, since TDP is expected to represent the equilibrium state of the supergiant, polarization modulation due to TDP should not change from orbit to orbit. Since mean polarization changed by only $< 0.05\%$ over their 10 month time interval, DT92 claim that the changes in polarization curves over this interval are due neither to changes in TDP nor interstellar polarization. They attribute this change to stochastic processes in the system and assert that TDP must therefore not be the dominant source of polarization. This agrees with the calculations of Bochkarëv et al. (1986), above.

Wolinski et al. (1996, hereafter W96) observe Cygnus X-1 over one orbit in U band with the High Speed Photometer on the Hubble Space Telescope. They note that the polarization spectrum in the ultraviolet departs significantly from the interstellar relation of Serkowski et al. (1975), which indicates that polarization in this wavelength regime is intrinsic to the binary. Indeed, the amplitude

of polarimetric variability versus wavelength is well-approximated by the addition of wavelength-dependent Rayleigh scattering and wavelength-independent Thomson scattering. While Thomson scattering is explained by free electrons in the circumbinary envelope, Rayleigh scattering results from neutral material in the accretion stream. Such neutral material has been observed in Cygnus X-1 (Mason et al. 1974, Kitamoto et al. 1984), HD 153919 (White et al. 1983), and Vela X-1 (Kallman & White 1982).

Of their thirteen observations of Cygnus X-1, the last one was taken one full phase later than initial observations. This point differs insignificantly from the first observations in Stokes Q, but Stokes U decreases from $U \approx 5\%$ to $U \approx 3.75\%$ over the 5.6 day period. This stochastic variation is comparable to the amplitude of orbital modulation. In order to obtain a fit to the BME model acceptable at $> 5\%$ significance, W96 must reject the observation at the end of the run. This fit implies an inclination of $i = 85°$ for Cygnus X-1 (no uncertainty is provided), which is unphysical. However, the amplitudes of variation in the Stokes Q and U data are $\Delta Q = 0.5\%$ and $\Delta U \approx 1\%$, while the amplitudes of the fits are $\Delta Q_{\rm fit} \approx 1\%$ and $\Delta U_{\rm fit} \approx 1.5\%$, respectively. Indeed, Cygnus X-1 is certainly not phase locked over even two orbits, which is one of the assumptions of the BME model. Thus, the observations of W96 cast doubt that the BME model is an accurate representation of the U band variability of the system.

W96 also observe the polarimetric variability of HD 153919 (eclipsing, O6f + neutron star binary) and Vela X-1 (eclipsing, B0.5Ib + neutron star X-ray binary) in U band. Data taken one full phase apart on Vela X-1, a nine-day time interval, differ by $\Delta Q, U \approx 4\%$ in both Stokes Q and U. However, the amplitude of variability is only $\Delta Q, U \approx 2\%$. Furthermore, both HD 153919 and Vela X-1 exhibit strong changes in polarization near phase 0.25 (first quadrature). This effect is twice the amplitude for HD 153919 in both Stokes Q and U ($\Delta Q = 2.5\%$ and $\Delta U = 1\%$), while it is equal to the Stokes Q amplitude and twice the Stokes U amplitude for Vela X-1 ($\Delta Q, U = 4\%$). The fact that this effect occurs at the same phase for both binaries with neutron star companions leads W96 to suggest an additional source of scattering in these systems.

Even after rejecting inconsistent observations on Vela X-1, W96 are unable to acceptably fit data in the F327M filter at $> 5\%$ significance. Therefore, the BME method fails for ultraviolet observations of Vela X-1. Rejecting inconsistent observations, W96 find an inclination of $i = 85°$ for HD 153919, which is consistent with prior estimates (Table 4.3). However, we caution that both

biases inherent to the BME inclination inversion method, resulting from noise as well as from tidal distortion polarization of the visible companion, act to increase inclination estimates. We measure a similar, high inclination for the non-eclipsing Cygnus X-1 that other polarimetrists measure for eclipsing systems. Indeed, all polarimetrically derived inclinations in Table 4.3 are higher than those derived using other methods. Thus, we claim that high inclinations derived polarimetrically are not independent checks of orbital inclination for high-inclination systems.

4.5.6 Disk Precession

Karitskaya & Bochkarev (1989) fit the lightcurve of Kemp et al. (1987), collected on 1,912 nights over a 4,500 night span, in the context of an inclined, precessing accretion disk to obtain an orbital inclination of $i = 60 \pm 5^\circ$ and disk obliquity $i_{\rm disk} = 17.5 \pm 2.5^\circ$. This value is consistent with the Ibragimov et al. (2007) determination of $i_{\rm disk} = 15 \pm 7^\circ$ from the precessional modulation of radio and X-ray emission, although they assume $i = 37.5 \pm 7.5^\circ$. However, Brocksopp et al. (1999a) derive a value of $i_{\rm disk} = 37^\circ$ from precessional modulation of X-rays, but they provide no estimate of uncertainty on this value.

Bruevich et al. (1978) suggest that the blackbody radiation from the disk in addition to reprocessing of X-rays brings the disk emission to $B_{\rm disk} = 0.03$ and $V_{\rm disk} = 0.04$ mag. Indeed, a sudden fading event of the system by $\Delta V = 0.04$ mag from the expected ellipsoidal lightcurve over one week has been interpreted as the disappearance and reappearance of the accretion disk (Karitskaya & Goranskij 1996). Delays in optical and X-ray flares have also been observed to span one to two weeks (Karitskaya et al. 2000, 2001). These results indicate the timescale between the deposition of material onto the disk (by the focused stellar wind) and accretion of that material by the black hole may be one to two weeks.

Disk loss is not uncommon in X-ray binaries, as the $\Delta V \approx 0.6$ mag decrease in flux from X Per from 1989 to 1990 is interpreted to be caused by disk loss (Norton et al. 1991, Fabregat et al. 1992). The correlation between decrease in flux and decrease in net polarization of the system during this period ($\Delta P \approx -0.5\%$) shows that the polarization from an accretion disk can be large indeed (Roche et al. 1997).

4.5.7 Quasi-Periodic Oscillation Scaling

Titarchuk & Fiorito (2004, hereafter TF04) show that an accretion disk revolving about the black hole at the Keplerian frequency will transition to sub-Keplerian rotation at a particular radius. This radius will be proportional to the Schwarzschild radius, which is proportional to the mass of the black hole. The normal mode oscillation of this bounded, sub-Keplerian region will be at a frequency inversely proportional to the radius of the sub-Keplerian region. Thus, TF04 suggest that the power spectrum of quasi-periodic oscillations of black holes will be related to black hole mass. They further suggest that the scaling of this power spectrum between two black holes is equal to the mass ratio of those objects.

Shaposhnikov & Titarchuk (2007, hereafter ST07) utilize this technique to verify the mass of the GRS 1915+105 black hole from the known mass of GRO J1655 − 40. Using the mass estimate of GRO J1655 − 40 of $M_{\rm J1655} = 6.3 \pm 0.5\ M_\odot$ from ellipsoidal modulation (Greene et al. 2001), ST07 determine the mass of GRS 1915+105 to be $M_{1915} = 15.6 \pm 1.5\ M_\odot$. This value is consistent with the estimate of Greiner et al. (2001, hereafter G01), where $M_{1915} = 14 \pm 4\ M_\odot$. G01 deduce an inclination of $i_{1915} = 70 \pm 2^\circ$ from the Doppler shifts of the jet and counterjet. Since this inclination has been observed to be stable for years, the precession period of the GRS 1915+105 accretion disk must be long. Therefore, the accretion disk must have obliquity $\delta_{1915,\rm disk} \approx 0^\circ$, indicating $i_{1915} \approx i_{1915,\rm disk}$.

Buoyed by the successful prediction of the mass of the GRS 1915+105 black hole, ST07 apply the QPO scaling technique to Cygnus X-1. They determine a mass of $M_{\rm CygX\text{-}1} = 8.7 \pm 0.8\ M_\odot$, which confirms its suspected black hole status. From the mass estimate of ST07, the radial velocity-derived mass ratio (G03), and a self-consistent analysis of the orbital dynamics of the binary, Iorio (2007, hereafter I07) derive an inclination of $i = 48.0 \pm 6.8^\circ$ for Cygnus X-1. They also determine the semimajor axis to be $a = 42 \pm 9\ R_\odot$, the supergiant radius to be approximately equal to the Roche lobe radius $R_{\rm star} = 21 \pm 6\ R_\odot$, and the supergiant mass to be $M_{\rm star} = 24 \pm 5\ M_\odot$.

This mass is inconsistent with the estimate of $M_{\rm star} = 17.8\ M_\odot$ from Herrero et al. (1995), who assumed an inclination of $i = 35^\circ$ and a radius of $R_{\rm star} = 17\ R_\odot$. The supergiant mass estimate from I07 is also inconsistent with $M_{\rm star} = 40 \pm 5\ M_\odot$ from Ziólkowski (2005), whose result depended on the effective temperature of and distance to the supergiant. Since the QPO scaling technique is independent of such assumptions, and since it accurately reproduced the mass of GRS 1915+105,

I07 claim that the $M_{\rm CygX\text{-}1} = 8.7 \pm 0.8\ M_\odot$ estimate from ST07 and their own $i = 48.0 \pm 6.8^\circ$ estimate are correct.

4.6 Discussion

Our high signal to noise data remove any possibility that single-orbit inclination estimates derived using BME model fitting to polarimetric data of Cygnus X-1 can be reconciled with those from eclipse studies, ellipsoidal modulation, and radial velocity tomography. Furthermore, such single-orbit inclination estimates cannot represent the true inclination of the system, because the lack of strong X-ray eclipses provides an upper limit of $i < 65^\circ$. Our derived inclinations, from two orbits spaced ten months apart, are inconsistent with this upper limit at the $4\sigma - 5\sigma$ level.

To determine the efficacy of the BME model when data are phase-binned over many orbits, we construct mean polarization curves from K80, DT89, and our observations. The Stokes Q and U axes in DT89 are the same as in our observations; namely, Q points north-south on the sky, and U is oriented northeast-southwest. However, K80 define their Stokes Q axis at a position angle of 95°. Therefore, we rotate their Stokes curves ($Q'_{\rm K}$ and $U'_{\rm K}$) by -95°:

$$Q_{\rm K} = Q'_{\rm K} \cos 190^\circ - U'_{\rm K} \sin 190^\circ \tag{4.12a}$$

$$U_{\rm K} = Q'_{\rm K} \sin 190^\circ + U'_{\rm K} \cos 190^\circ. \tag{4.12b}$$

Next, we re-wrap the curves of K80 and DT89 to the ephemeris used in our fits, which is from Gies et al. (2003: G03). From the ephemerides listed in Table 4.2, we derive the following conversions between the phases of K80 ($\phi_{\rm K}$), DT89 ($\phi_{\rm DT}$), and G03 (ϕ):

$$\phi = (1 + 3.05 \times 10^{-5})\phi_{\rm K} - 0.137 \tag{4.13a}$$

$$\phi = (1 - 1.59 \times 10^{-5})\phi_{\rm DT} - 7.17 \times 10^{-3}. \tag{4.13b}$$

We construct the mean polarization curves from both of our observing runs. This is equivalent to taking the mean for each q_i and u_i amplitude parameter in Table 4.2. Figure 4.8 shows the

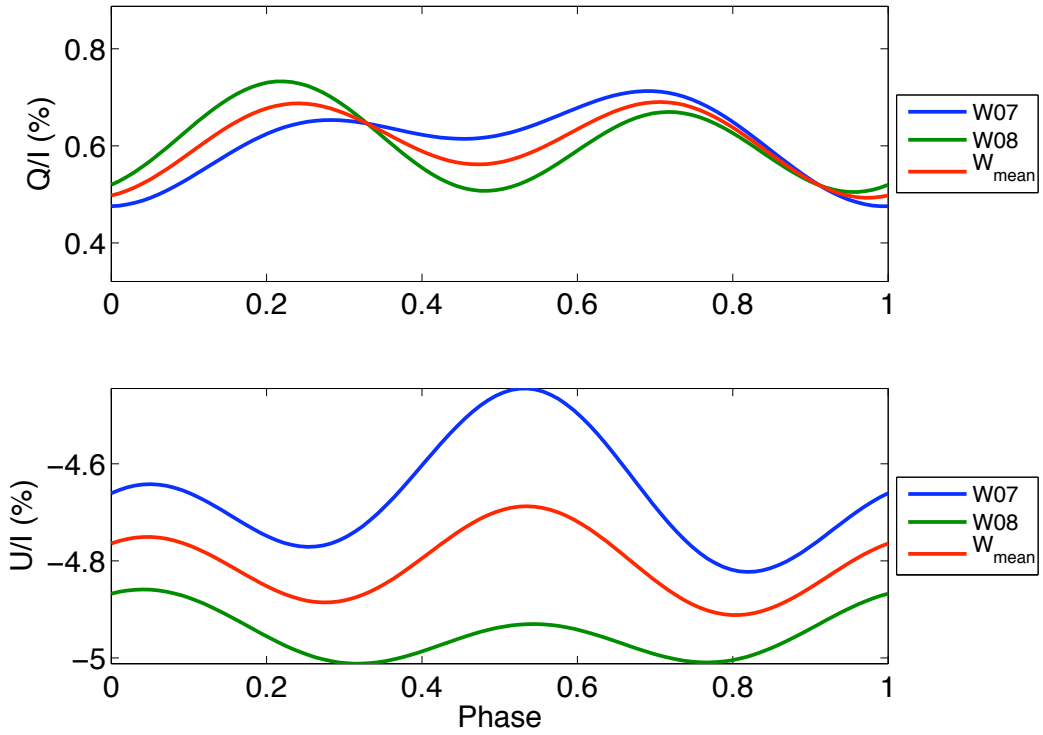

Figure 4.8: Polarimetric modulation observed in Aug 2007 and Jun 2008. The mean modulation from the two runs is also shown.

polarization curves from both runs as well as the curves obtained when taking their mean. We now take the mean Q, U versus phase across the data sets. Individual Q, U versus phase curves and their mean are shown in Figure 4.9. Plotting U versus Q throughout the orbit is used in the literature to get a sense of the distribution of scatterers as well as the presence of eclipses. While we do not use these curves to suggest the nature of the scattering, we nevertheless plot them in Figure 4.10. Our data show the strongest departure from ellipticity in the (Q, U) plane, which is explained by the fact that our data possess the largest ratio of the first to the second harmonic amplitudes of all three datasets ($p_{\rm I}/p_{\rm II}$ in Table 4.2). The K80 curves are re-wrapped to our ephemeris and rotated to our coordinate system, while the DT89 curves are re-wrapped to our ephemeris.

We then fit the mean curves according to Equations 4.4a and 4.4b, derive inclination from Equations 4.5a and 4.5b, and determine the position angle of the line of quadratures from Equations 4.6a through 4.6g. In addition, we re-derive these results from K80 and DT89 data (Table 4.2). With the addition of the K80 and DT89 data sets to our data (the "All" column in Table 4.2), we find that the inclination estimates decrease to the maximum allowable inclination set by the lack of observed X-ray eclipses. It is therefore tempting to speculate that the inclusion of all three data sets

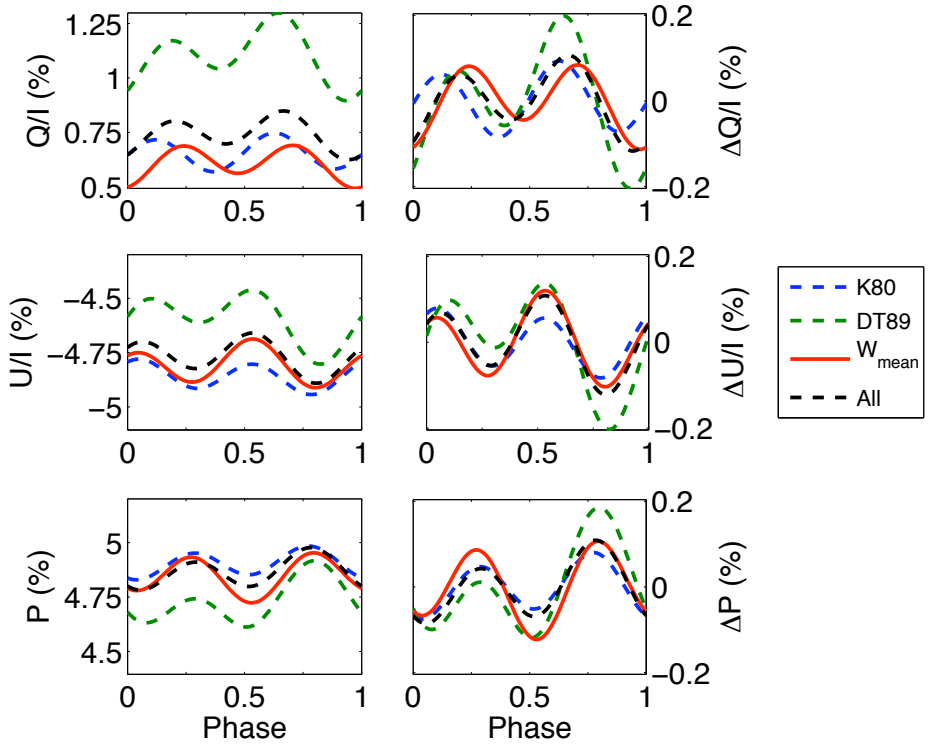

Figure 4.9: Cygnus X-1 polarimetric modulation from Kemp (1980: K80), Dolan & Tapia (1989: DT89), mean modulation from this work (W_{mean}), and mean modulation between all three data sets ("All"). Note the difference in scaling between absolute (Q, U, P) and relative $\Delta(Q, U, P)$ polarization.

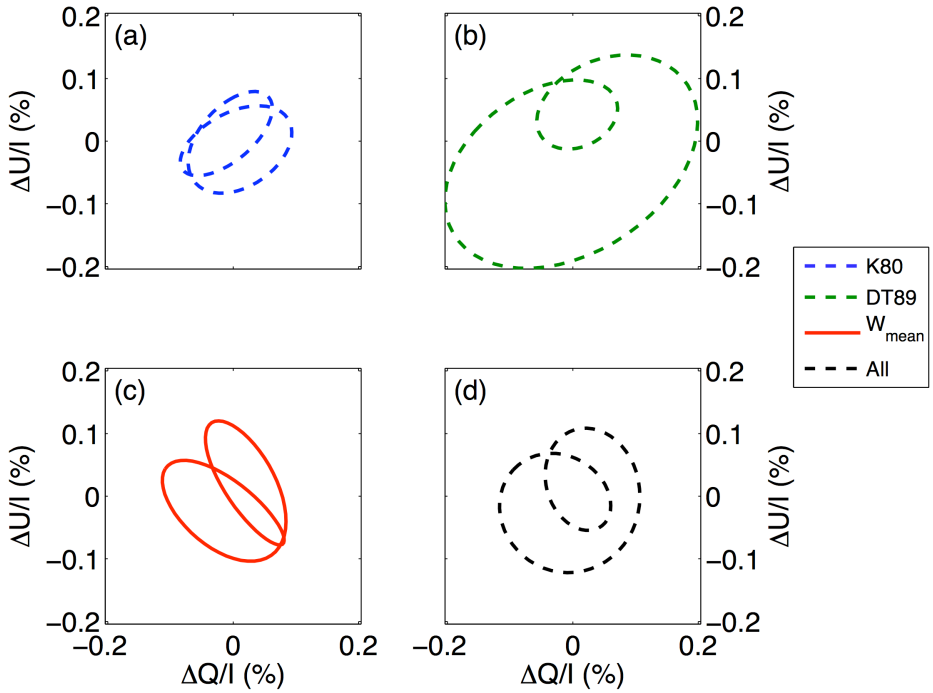

Figure 4.10: U versus Q for the data sets in Figure 4.9.

Table 4.4: Photometric, Precessional Modulation

Reference	MJD Range	$\Delta B_{\rm orb}$ (mmag)	$\Delta B_{\rm prec}$ (mmag)	$\Delta B_{\rm orb}/\Delta B_{\rm prec}$
Kemp et al. (1987)	$42655 - 45318$	48(3)	9.5(2.0)	5.1(1.1)
Brocksopp et al. (1999a)	$50240 - 51100$	28.60(78)	16.409(29)	1.733(47)

has averaged out stochastic changes in the polarization of Cygnus X-1 and produced the "mean" state of the system, which evidently lies near the maximum allowable inclination. However, it is unlikely that the addition of only three orbits to the ≈ 100 from K80 should unveil such a pristine mean state, regardless of the quality of those extra orbits. Since the overwhelming data set of K80 produces an unacceptably high inclination, due to lack of eclipses, we must conclude that the mean polarization curves from an arbitrary number of orbits cannot uncover a physically meaningful inclination estimate.

We are therefore left with the conclusion that the BME method fails in determining the inclination of Cygnus X-1, regardless of the combination of telescope aperture and observing duration. This is perhaps not surprising when the high degree of complexity of the system, with each part contributing to the total polarization signature, is considered:

(1) The supergiant is tidally distorted

(2) The circumbinary envelope is ionized

(3) The focused stellar wind consists of ionized, Thomson scatterers and neutral, Rayleigh scatterers

(4) The size of the accretion disk changes during the low/hard and high/soft states, and it may disappear altogether over an entire orbit

(5) The strength of the focused stellar wind, the degree of ionization of all parts of the system, and the frequency of flaring change during the low/hard and high/soft states

(6) The optical ellipsoidal modulation disappears (Brocksopp et al. 1999a) or becomes single-peaked (Voloshina et al. 1997) in the high/soft state

(7) The accretion disk is inclined and precessing, and the dominant precession period is not stable on decadal timescales

(8) The accretion disk rim likely contains a hot spot that is subject to flaring

Table 4.4 lists orbital and precessional modulation of the system photometry roughly 15 years

apart. There appears to be a significant increase in the amplitude of the precessional modulation compared to the orbital, ellipsoidal modulation between 1982 and 1996. This implies that either the accretion disk became brighter, the supergiant became fainter, or both occurred in this time interval. Karitskaya et al. (2006, hereafter K06) observe dimming of the system by $\Delta U = 65 \pm 3$, $\Delta B = 31 \pm 3$, and $\Delta V = 29 \pm 3$ mmag from 1997 to 2004. They also report cooling of the photosphere by $\Delta T_{\rm eff} \approx 1{,}400$ K (from the HeI λ4713Å line), from $T_{\rm eff} = 31{,}800 \pm 500$ K to $T_{\rm eff} = 30{,}400 \pm 500$ K, during this interval. Additionally, K06 show an increase in X-ray emission during the stellar dimming.

K06 interpret these observations in terms of a $\Delta R/R \approx 1 - 2\%$ increase in radius and resultant photospheric cooling. The increased radius increases accretion onto the black hole due to increased Roche lobe overflow. In addition, the lower photospheric temperature decreases the velocity of the radiatively-driven, focused stellar wind, which allows for more efficient accretion. A higher accretion rate is expected to increase the optical luminosity of the black hole due to increased X-ray reprocessing and inward migration of the inner radius of the accretion disk. Thus, the observations of Brocksopp et al. (1999a) were taken during a time when the supergiant was dimming and the accretion disk was brightening.

The accretion disk rotates by $\approx 360^\circ$ over one orbit about the angular momentum axis of the binary, since the precession period is much longer than the orbital period. Scattering of optical flux from the supergiant by the accretion disk therefore produces photometric and polarimetric modulation at the orbital frequency. Bochkarev & Karitskaya (1988a, hereafter BK88) model the amplitude of the polarimetric variability of the disk to be $\Delta P_{\rm disk} \approx 0.25\%$, which is comparable to the observed variability of the system. However, Kemp et al. (1983, hereafter K83) observe the 294 day precessional period of the accretion disk in polarized light to only have amplitude $\Delta P_{\rm disk} \approx 0.05\%$ from 1975 to 1983. This amplitude is 1/5 of that predicted by BK88.

BK88 further model that the second harmonic amplitude due to the disk should be $p_{\rm II,disk} = 0.11\%$, and that the ratio of amplitudes of the first and second harmonics should be $(p_{\rm I}/p_{\rm II})_{\rm disk} = 0.8$ for disk obliquity $i_{\rm disk} < 20 - 30^\circ$. The observations of K80 exhibit $p_{\rm I}/p_{\rm II} = 0.24$ (Table 4.2), which is 1/3 of that calculated by BK88 for significant disk polarization. BK88 calculate the polarimetric variability of scattering by the accretion disk to therefore contribute $< 25 - 50\%$ of the observed variability. However, the observations of DT89 as well as our own (W07 and W08) show the strength

of the first harmonic to be $p_{\rm I}/p_{\rm II} > 0.8$ since June 1988, which is consistent with scattering by the accretion disk.

It should be noted that our W08 data set shows a first harmonic amplitude half of this value (Table 4.2), but the BME fit does not accurately model the large first harmonic modulation observed. That is, the zeroth through second order BME fit in Figure 4.2 underestimates the strength of the modulation near phase 0.05. Indeed, adding the $\Delta U \approx 0.05\%$ difference between model and data to $u_{\rm I}$ gives a ratio of $p_{\rm I}/p_{\rm II} = 0.81$. This suggests that the fractional polarization of the accretion disk increased during the 1980s and that it is currently significant. This is corroborated by the above result that the relative flux of the accretion disk has increased during that interval: the amplitude of photometric, precessional modulation is more than half the amplitude of photometric, orbital modulation. Since the dominant precessional period of the accretion disk also changed during this time (section 4.2.2), it appears the 1980s saw drastic changes in the accretion disk.

Cygnus X-1 is not the only high mass X-ray binary for which accretion disk polarization has been observed. Efimov et al. (1984) observe polarimetric modulation of the A7Ib supergiant/neutron star system SS 433 at both the 13 day orbital period as well as the 164 day precessional period of the inclined accretion disk. They observe the ratio of first to second harmonic amplitudes to be $p_{\rm I}/p_{\rm II} \approx 2.5$. This indicates that the contribution of the accretion disk polarization is significant.

We also observe an increase in mean polarization from $p_0 \equiv \sqrt{q_0^2 + u_0^2} = 4.71\%$ to $p_0 = 4.99\%$ (Table 4.2) in the ten months between the Aug 2007 and Jun 2008 runs. This $\Delta p_0 \approx 0.3\%$ increase is comparable to the amplitude of polarimetric orbital modulation. This is in contrast to the observations of K79, who observe a linear increase in mean system polarization of 1.8×10^{-6} per day, or an increase of only $\approx 0.06\%$ in ten months. Indeed, Dolan & Tapia (1992) also observe a change in mean polarization of only $\approx 0.05\%$ in the ten months between their observations (Sep 1987 to Jul 1988). However, they report that the amplitude of Stokes Q variability tripled in those ten months, while the amplitude in Stokes U was halved. Indeed, a χ^2 analysis of the two data sets shows them to be consistent at the $\alpha < 10^{-5}$ level of significance. Our Jun 2008 data are inconsistent with the polarization curves from the Aug 2007 observations: $\alpha_Q = 0$ ($\chi^2/n = 197/14$) and $\alpha_U = 0$ ($\chi^2/n = 2,721/14$). Thus, we confirm that the Cygnus X-1 system changes dramatically over a ten month time interval (≈ 50 orbits). It should be noted that the observations at phase 0.13 in Figure 4.2 correspond to the next orbit of the system, yet they appear to be consistent with the

observations from the first orbit. Therefore, we have weak evidence that the phase-locking of the system occurs over one to two orbits.

If the secular increase in system polarization seen by K79 is from variability in the ISM, one must conclude that the order of magnitude larger secular variability in our data is due to stochastic changes in the intrinsic polarization of the system. It is therefore likely that the degree of polarization of either the accretion stream, accretion disk, or both have increased in ten months. It is expected that ≈ 2.1 precessional periods, with 147 day period, have progressed in this time interval. The precessional phase of the accretion disk, and therefore the inclination of the disk to the line of sight, is expected to be similar between the two runs. Therefore, if the secular variability observed is due to the accretion disk, it must represent a change in the accretion disk as opposed to precession.

Given that the accretion disk represents a significant fraction of the polarimetric variability of Cygnus X-1, fluctuations in the disk are likely the cause of the stochastic noise seen by other polarimetrists. Bochkarev et al. (1998, hereafter B98) observe two large flares of $\Delta V_{\rm flare} = 0.04$ mag of order one day duration coincident with dips in X-ray emission by 20%. Another flare exhibited a brightening in the UBV bands of $\Delta U_{\rm flare} = 0.12$, $\Delta B_{\rm flare} = 0.12$, and $\Delta V_{\rm flare} = 0.02$. They assume this to be from optically thin hydrogen gas at $T = 20{,}000 \pm 10{,}000$ K, which indicates a hot spot in the accretion disk. The X-ray dips are thought to arise when the hot spot eclipses the X-ray source near the center of the disk (Karitskaya et al. 2000).

Poutanen et al. (2008, hereafter P08) observe the distribution of X-ray dips, of order one minute duration, versus disk precessional phase. Precessional phase $\Phi \equiv 0$ when the disk flux is at a minimum, and the precession period is now 151.43 days (Lachowicz et al. 2006). At precessional phase $\Phi = 0$, the disk is therefore closest to edge-on, and it is closest to face-on at $\Phi = 0.5$. P08 observe the X-ray dip distribution to peak at $\Phi \approx 0.05 - 0.1$, which is consistent with X-ray source occultation by a bulge located between the supergiant and black hole. The formation of the bulge at the disk rim results from the accretion stream impacting the disk, and P08 model the bulge location to lag behind the supergiant (as seen by the black hole), by $\phi_{\rm bulge} \approx 25^\circ$. As the disk precesses, the bulge moves up and down, perpendicular to the orbital plane. This explains why dips are strong at precessional phase $\Phi \approx 0$ and weak at $\Phi \approx 0.5$. Occultation in the disk correlated with precessional phase is also suggested by optical polarimetric observations. Indeed, Kemp et al. (1983: K83) suggest that the non-sinusoidal modulation is caused by partial eclipsing of the polarized light from the disk at certain precessional phases.

Therefore, the perhaps *ad hoc* suggestion by Kemp et al. (1979: K79) of an occulted, scattering spot located at the intersection of disk and accretion stream (section 4.5.5) now seems to have some merit. However, it should be noted that this model was suggested on the basis of the non-elliptical locus in (Q, U) space from K79, which appears similar to our own data (Figure 4.10c). As noted before, Simmons et al. (1980: S80) successfully fit the data of K79 by the BME model without requiring the scattering spot of K79. However, the BME model does not accurately represent the physical state of Cygnus X-1, and the scattering spot model may still have some merit in light of the observations of DT89 as well as our own.

In addition to disk occultation on the precessional period, there is a wealth of evidence that X-ray dips also occur near orbital phase $\phi \approx 0$, when the black hole is in superior conjunction (Li & Clark 1974; Mason et al. 1974; Parsignault et al. 1976a, b; Pravdo et al. 1980; Remillard & Canizares 1984; Kitamoto et al. 1989; Balucinska-Church et al. 2000; Feng & Cui 2002; P08). The occulting material in this case is thought to be neutral material in the accretion stream. Kitamoto & Miyamoto (1984, hereafter KM84) observe the X-ray spectrum of the source during an X-ray dip in the low/hard state, and they see the K-absorption edge of iron at $E = 7.18 \pm 0.18$ keV (90% confidence interval). This is interpreted to arise from weakly ionized Fe VI or less, implying a temperature of $T < 30{,}000$ K. This suggests most elements present in the stream are effectively neutral. The decrease in orbital, polarimetric modulation with increasing wavelength observed by Wolinski et al. (1996: W96, see section 4.5.5) suggests that such neutral material in the accretion stream comprises a significant component to the polarimetric variability of the system.

Absence of the iron emission line implies a small occulting blob size, and KM84 estimate it to be of order $d_{\rm blob} = 10^9$ cm in length. The presence of short X-ray dips, of $t \approx 2$s duration, suggests an upper limit to the size of the X-ray source of $d_{\rm X\text{-}ray} < 4 \times 10^8$ cm. Ibragimov et al. (2005) fit the X-ray spectrum for column density and find that it increases near orbital phase $\phi = 0$. This result adds weight to the theory that X-ray dips at superior conjunction of the black hole are due to occultation of the X-ray source by the focused stellar wind. Therefore, Brocksopp et al. (1999a, hereafter B99) suggest that the observed orbital modulation of radio and X-ray emission is due to absorption by the focused stellar wind, while the ultraviolet, optical, and near-IR modulation is due to the ellipsoidal modulation of the supergiant (section 4.2.2).

The complexity in the Cygnus X-1 system is very high, even during the fiducial low/hard state.

During the high/soft state, additional events are introduced. Natali et al. (1978) observe photometric flickering of $\Delta V = 0.06 - 0.10$ mag over ≈ 30 min timescales during this state, which is one to two times the strength of the orbital, ellipsoidal modulation. One might therefore expect the polarimetric flickering during the high/soft state to be dramatic.

The disappearance of observed orbital modulation in the radio and X-rays during this state (B99), as well as the single-peaked (Voloshina et al. 1997) or nonexistent (B99) optical lightcurve, suggest that dramatic changes in Cygnus X-1 occur in the high/soft state. On the grounds that the photometric contribution of the accretion disk is only $\approx 3\%$ during the low/hard state (Bruevich et al. 1978, see section 4.5.6) B99 claim that the increased optical output in the high/soft state is not completely due to a brighter accretion disk. They suggest that the hemisphere of the supergiant facing the black hole as well as the accretion stream become brighter due to increased irradiation by the X-ray source. The absence of orbital modulation in the radio is attributed to the disappearance of jets, while increased X-ray flaring overwhelms the orbital modulation in X-rays.

4.7 Conclusion

The enhanced sensitivity to asymmetry in a system from polarimetry over photometry provides geometric information that is difficult to determine with any other method. However, the exorbitant number of free parameters, and the large number of significant and variable polarization sources in Cygnus X-1, causes difficulty in polarimetric modeling of the system. Others have claimed that the scattering model of Brown et al. (1978: BME) can accurately determine the inclination of binary systems from polarimetry. These claims generally result from the agreement of BME-derived inclinations with inclinations derived from eclipses. However, we note that inclinations derived by this model are systematically higher (towards edge-on geometries) than those determined by other methods. Therefore, the true inclination of eclipsing binaries will be derived from the BME model simply from biases in the model.

Cygnus X-1 inclinations determined both by monitoring of order 100 orbits with a small telescope and large telescope monitoring of individual orbits are consistently higher than allowed by the lack of X-ray eclipses. Therefore, the scattering model of BME is not applicable to the Cygnus X-1 system, and it may not be applicable to most binary systems as well. Previous authors have attributed the

failure of the BME model to produce physically plausible inclinations to low signal-to-noise data. However, our high precision observations (night-to-night polarimetric precision of one part in 10^4) refute this hypothesis: the BME model cannot produce the true inclination of the system, regardless of the number of nights and telescope aperture.

The critical assumptions of the BME model are single scattering in a phase-locked system. Our observations spaced ten months apart confirm the finding by Wolinski et al. (1996) that the polarization of the Cygnus X-1 system varies on orbital timescales. Indeed, phase-locking of similar systems is also known to occur over one to ten orbits (Dolan & Tapia 1984, 1988). The cause of this stochastic variability is unknown, but variable accretion rate and flaring in the Cygnus X-1 disk contribute significantly. Scattering of the flux from the supergiant by the optically thick accretion disk, which is inclined and precessing with a 147 day period, must also contribute to the long-term variability of the system. Indeed, the precession period and brightness of the accretion disk also seem to be variable on decadal timescales.

It is unlikely that polarimetry will meaningfully constrain the mass of the black hole in Cygnus X-1. A more promising method is the scaling of quasi-period oscillation (QPO) frequency between this black hole and others of known mass (Titarchuk & Fiorito 2004). Indeed, Shaposhnikov & Titarchuk (2007) have successfully predicted the mass of the GRS 1915+105 black hole with this technique, and they estimate the black hole in Cygnus X-1 to be $M_{\rm BH} = 8.7 \pm 0.8\ M_\odot$. However, the failure of polarimetry in determining the mass of black holes in high mass X-ray binaries results from the fact that they are too sensitive to asymmetry in the system. When applied to extrasolar planets, polarimetric monitoring provides geometric information that cannot be determined from other methods. The future of polarimetry in this field looks bright indeed. In an attempt to describe the atmospheres of extrasolar planets, the next chapter investigates the stability of liquid water oceans in so-called "hot Neptunes".

References

Abubekerov, M. K., Antokhina, E. A., & Cherepashchuk, A. M. 2004, Astron. Rep. 48, 550.

Albert, J., Aliu, E., Anderhub, H., Antoranz, P., Armada, A., Baixeras, C., Barrio, J. A., Bartko,

H., Bastieri, D., Becker, J. K., Bednarek, W., Berger, K., Bigongiari, C., Biland, A., Bock, R. K., & 125 coauthors. 2007, ApJ 665, L51.

Angel, J. R. P. 1969, ApJ 158, 219.

Aspin, C. & Simmons, J. F. L. 1982, MNRAS 199, 601.

Aspin, C., Simmons, J. F. L., & Brown, J. C. 1981, MNRAS 194, 283.

Avery, R. W., Stokes, R. A., Michalsky, J. J., & Ekstrom, P. A. 1975, AJ 80, 1026.

Balog, N. I., Goncharskii, A. V., & Cherepashchuk, A. M. 1981, SvA 25, 38.

Balona, L. A., Egan, J., & Marang, F. 1989, MNRAS 240, 103.

Balucinska-Church, M., Belloni, T., Church, M. J., & Hasinger, G. 1995, A&A 302, L5.

Balucinska-Church, M., Church, M. J., Charles, P. A., Nagase, F., LaSala, J. & Barnard, R. 2000, MNRAS 311, 861.

Barrett, P. 1996, PASP 108, 412.

Batten, A. H. 1967, Pub. Dom. Ap. Obs. 13, 8.

Berdyugin, A. & Piirola, V. 2002, A&A 394, 181.

Bochkarev, N. G. & Karitskaya, E. A. 1988a, Adv Sp Res 8, 205 (BK88).

Bochkarev, N. G., Karitskaya, E. A., & Shakura, N. I. 1975, SvAL 1, 118.

Bochkarev, N. G., Karitskaya, E. A., Syunyaev, R. A., & Shakura, N. I. 1979, SvAL 5, 99.

Bochkarëv, N. G., Karitskaya, E. A., Loskutov, V. M. & Sokolov, V. V. 1986, SvA 30, 43.

Bochkarev, N. G., Karitskaya, E. A., & Lyuty, V. M. 1998, IAU Symp. 188, 384 (B98).

Bolton, C. T. 1972, Nature 235, 271.

Bolton, C. T. 1975, ApJ 200, 269.

Bondi, H. & Hoyle, F. 1944, MNRAS 104, 273.

Brocksopp, C., Fender, R. P., Larionov, V., Lyuty, V. M., Tarasov, A. E., Pooley, G. G., Paciesas, W. S., & Roche, P. 1999a, MNRAS 309, 1063 (B99).

Brocksopp, C., Tarasov, A. E., Lyuty, V. M., & Roche, P. 1999b, A&A 343, 861.

Brown, J. C., McLean, I. S., & Emslie, A. G. 1978, A&A 68, 415 (BME).

Bruevich, V. V., Kilyachkov, N. N, Syunyaev, R. A., & Shevchenko, V. S. 1978, SvAL 4, 292.

Castor, J. I., Abbott, D. C., & Klein, R. I. 1975, ApJ 195, 157.

Cherepashchuk, A. M. 1975, SvA 19, 47.

Daniel, J. Y. 1980, A&A 86, 198.

Daniel, J.-Y. 1981, A&A 94, 121 (D81).

Davis, A. B., Moffat, A. F. J., & Niemela, V. S. 1981, ApJ 244, 528.

Davis, R., & Hartmann, L. 1983, ApJ 270, 671.

De Greve, J. P., Hellings, P., & van den Heuvel, E. P. J. 1988, A&A 189, 74.

Di Salvo, T., Done, C., Zycki, P. T., Burderi, L., & Robba, N. R. 2001, ApJ 547, 1024.

Dolan, J. F. 1984, A&A 138, 1.

Dolan, J. F. & Tapia, S. 1984, A&A 139, 249.

Dolan, J. F. & Tapia, S. 1988, A&A 202, 124.

Dolan, J. F. & Tapia, S. 1989, ApJ 344, 830 (DT89).

Dolan, J. F. & Tapia, S. 1992, ApJ 384, 249 (DT92).

Dolan, J. F., Coe, M. J., Crannell, C. J., Dennis, B. R., Frost, K. J., Orwig, L. E., & Caraveo, P. 1979, Nature 280, 126.

Drissen, L, Lamontagne, R., Moffat, A. F. J., Bastien, P. & Seguin, M. 1986a, ApJ 304, 188.

Drissen, L, Moffat, A. F. J., Bastien, P., Lamontagne, R., & Tapia, S. 1986b, ApJ 306, 215.

Efimov, Y. S., Piirola, V., & Shakhovskoy, N. M. 1984, A&A 138, 62.

Esin, A. A., Narayan, R., Cui, W., Grove, J. E., & Zhang, S.-N. 1998, ApJ 505, 854.

Fabregat, J., Reglero, V., Coe, M. J., Clement, R., Gorrod, M. J., Norton, A. J., Roche, P. D., Suso, J., & Unger, S. J. 1992, A&A 259, 522.

Fender, R. P., Stirling, A. M., Spencer, R. E., Brown, I., Pooley, G. G., Muxlow, T. W. B., & Miller-Jones, J. C. A. 2006, MNRAS 369, 603.

Feng, Y. X. & Cui, W. 2002, ApJ 564, 953.

Fosalba, P., Lazarian, A., Prunet, S., & Tauber, J. A. 2002, ApJ 564, 762.

Friend, D. B. & Castor, J. I. 1982, ApJ 261, 293.

Frontera, F., Palazzi, E., Zdziarski, A. A., Haardt, F., Perola, G. C., Chiappetti, L., Cusumano, G., Dal Fiume, D., Del Sordo, S., Orlandini, M., Parmar, A. N., Piro, L., Santangelo, A., Segreto, A., Treves, A., & Trifoglio, M. 2001, ApJ 546, 1027.

Gallo, E., Fender, R., Kaiser, C., Russell, D., Morganti, R., Oosterloo, T., & Heinz, S. 2005, Nature 436, 819.

Gehrels, T. 1972, ApJ 173, L23.

Gierliński, M., Zdziarski, A. A., Done, C., Johnson, W. N., Ebisawa, K., Ueda, Y., Haardt, F., & Philips, B. F. 1997, MNRAS 288, 958.

Gies, D. R. & Bolton, C. T. 1982, ApJ 260, 240.

Gies, D. R. & Bolton, C. T. 1986a, ApJ 304, 371.

Gies, D. R. & Bolton, C. T. 1986b, ApJ 304, 389.

Gies, D. R., Bolton, C. T., Thomson, J. R., Huang, W., McSwain, M. V., Riddle, R. L., Wang, Z., Wiita, P. J., Wingert, D. W., Csák, B., & Kiss, L. L. 2003, ApJ 583, 424 (G03).

Gnedin, Y. N. & Silant'ev, N. A. 1980, SvAL 6, 344.

Gnedin, Y. N., Borisov, N. V., Natsvlishvili, T. M., Piotrovich, M. Y., & Silant'ev, N. A. 2003, arXiv:0304158v1 (Gn 03).

Greene, J., Bailyn, C. D., & Orosz, J. A. 2001, ApJ 554, 1290.

Greiner, J. Cuby, J. G. & McCaughrean, M. J. 2001, Nature 414, 522 (G01).

Guinan, E. F., Dorren, J. D., Siah, M. J., & Koch, R. H. 1979, ApJ 299, 296.

Herrero, A. Kudritzki, R. P., Gabler, R., Vilchez, J. M, & Gabler, A. 1995, A&A 297, 556.

Hiltner, W. A. & Mook, D. E. 1966, ApJ 143, 1008.

Ho, C. & Arons, J. 1987, ApJ 316, 283.

Holt, S. S., Kaluzienski, L. J., Boldt, E. A., & Serlemitsos, P. J. 1976, Nature 261, 215.

Holt, S. S., Kaluzienski, L. J., Boldt, E. A., & Serlemitsos, P. J. 1979, ApJ 233, 344.

Horn, J., Hubert, A. M., Hubert, H., Koubsky, P., & Bailloux, N. 1992, A&A 259, L5.

Hutchings, J. B. 1974, ApJ 188, 341.

Hutchings, J. B. 1978, ApJ 226, 264.

Hutchings, J. B., Crampton, D., Glaspey, J., & Walker, G. A. H. 1973, ApJ 182, 549.

Ibragimov, A., Poutanen, J., Gilfanov, M., Zdziarski, A. A., & Shrader, C. R. 2005, MNRAS 362, 1435.

Ibragimov, A., Zdziarski, A. A., & Poutanen, J. 2007, MNRAS 381, 723.

Iorio, L. 2007, arXiv: 0707.3525 (I07).

Jensen, E. L. N. & Mathieu, R. D. 1997, AJ 114, 301.

Kallman, T. R. & White, N. E. 1982, ApJ 261, L35.

Karitskaya, E. A. 1979, Astron. Tsirk. No. 1088, 1.

Karitskaya, E. A. & Bochkarev, N. G. 1989, in Variable Phenomena in Close Binary Stars, Communications from the Konkoly Observatory of the Hungarian Academy of Sciences 10, No. 93, ed. L. Patkós (Budapest), p. 255.

Karitskaya, E. A. & Goranskij, V. P. 1996, IAU 4404, 1.

Karitskaya, E. A. & Goranskii, V. P., Grankin, K. N., & Mel'Nikov, S. Y. 2000, Astron Lett 26, 22.

Karitskaya, E. A., Voloshina, I. B., Goranskii, V. P., Grankin, K. N., Dzhaniashvili, É. B., Ezhkova, O. V., Kochiashvili, N. T., Kumsiashvili, M. I., Kusakin, A. V., Lyutyi, V. M., Mel'Nikov, S. Y.., Metlova, N. V. 2001, Astron Rep 45, 350.

Karitskaya, E. A., Lyuty, V. M., Bochkarev, N. G., Shimanskii, V. V., Tarasov, A. E., Bondar, A. V., Galazutdinov, G. A., Lee, B.-C., & Metlova, N. V. 2006, IAU 5678, 1 (K06).

Kartasheva, T. A. 2002b, Bull. Spec. Astrophys. Obs. 54, 56.

Kartje, J. F. & Königl, A. 1991, ApJ 375, 69.

Kemp, J. C. 1980a, ApJ 235, 595.

Kemp, J. C. 1980b, A&A 91, 108 (K80).

Kemp, J. C. 1983, IAU Circ. 3780.

Kemp, J. C. & Herman, L. C. 1977, ApJ 218, 770.

Kemp, J. C., Southwick, R. G., & Rudy, R. J. 1976, ApJ 210, 239.

Kemp, J. C., Barbour, M. S., Herman, L. C. & Rudy, R. J. 1978a, ApJ 220, L123 (K78).

Kemp, J. C., Herman, L. C., & Barbour, M. S. 1978b, AJ 83, 962.

Kemp, J. C., Barbour, M. S., Parker, T. E., & Herman, L. C. 1979, ApJ 228, 23 (K79).

Kemp, J. C., Barbour, M. S., Henson, G. D., Kraus, D. J., Nolt, I. G., Radostitz, J. V., Priedhorsky, W. C., Terrell, J., & Walker, E. N. 1983, ApJ 271, 65 (K83).

Kemp, J. C., Karitskaya, E. A., Kumsiashvili, M. I., Lyutyi, V. M., Khruzina, T. S., & Cherepashchuk, A. M. 1987, SvA 31, 170.

Khaliullina, A. I. & Khaliullin, K. F. 1981, SvA 25, 593.

Kitamoto, S. & Miyamoto, S. 1984, PASJ 36, 731 (KM84).

Kitamoto, S., Miyamoto, S., & Yamamoto, T. 1989, PASJ 41, 81.

Kitamoto, S., Egoshi, W., Miyamoto, S., Tsunemi, H., Ling, J. C., Wheaton, W. A., & Paul, B. 2000, ApJ 531, 546.

Kron, G. E. & Gordon, K. C. 1950, ApJ 111, 454.

Kruszewski, A. 1972, Acta Astron. 22, 405.

Lachowicz, P., Zdziarski, A. A., Schwarzenberg-Czerny, A., Pooley, G. G., & Kitamoto, S. 2006, MNRAS 368, 1025 (L06).

Lamontagne, R. & Moffat, A. F. J. 1987, AJ 94, 1008.

Lamontagne, R., Moffat, A. F. J., Drissen, L., Robert, C., & Matthews, J. M. 1996, AJ 112, 2227.

Leahy, D. A. & Ananth, A. G. 1992, MNRAS 256, 39.

Lester, D. F., Nolt, I. G., & Radostitz, J. V. 1973, Nature Phys. Sci. 214, 125.

Leung, K.-C., Moffat, A. F. J., & Seggewiss, W. 1983, ApJ 265, 961.

Li, F. K. & Clark, G. W. 1974, ApJ 191, L27.

Lipunova, N. A. 1982, SvAL 8, 128.

Lipunova, N. A. & Cherepashchuk, A. M. 1982, AZh 59, 73.

Long, K. S., Chanan, G. A., & Novick, R. 1980, ApJ 238, 710.

Luna, H. C. 1982, PASP 94, 695.

Lyutyi, V. M. 1985, SvA 29, 429.

Lyutyj, V. M., Sunyaev, R. A., & Cherepashchuk, A. M. 1973, SvA 17, 1.

Manchanda, R. K. 1983, Astrophys. Space Sci. 91, 455.

Manchanda, R. K. 2001, J. Astrophys. Astr. 22, 9.

Manset, N. & Bastien, P. 2001, AJ 122, 3453.

Manset, N. & Bastien, P. 2003, AJ 125, 3274.

Martin, P. G. 1974, ApJ 187, 461.

Mason, K. O., Hawkins, F. J., Sanford, P. W., Murdin, P., & Savage, A. 1974, ApJ 192, L65.

Massey, P. 1981, ApJ 244, 157.

Massey, P., & Conti, P. S. 1981a, ApJ 244, 169.

Massey, P. & Niemela, V. S. 1981, ApJ 245, 195.

Massey, P., Conti, P. S., & Niemela, V. S. 1981, ApJ 246, 145.

Mathewson, D. S. & Ford, V. L. 1970, Mem. RAS 74, 139.

McLean, I. S. 1980, ApJ 236, 149.

Merril, J. E. 1963, in *Photoelectric Astronomy for Amateurs*, ed. F. B. Wood. Macmillan, New York, p. 176.

Metzger, A. E. & Dolan, J. F. 1968, AJ 73, 107.

Michalsky, J. J. & Swedlund, J. B. 1977, ApJ 212, 221.

Michalsky, J. J., Swedlund, J. B., & Avery, R. W. 1975a, Nature 254, 39.

Michalsky, J. J., Swedlund, J. B., & Stokes, R. A. 1975b, ApJ 198, L101.

Milgrom, M. 1978, A&A 65, L1.

Miller, J. M., Fabian, A. C., Wijnands, R., Remillard, R. A., Wojdowski, P., Schulz, N. S., Di Matteo, T., Marshall, H. L., Canizares, C. R., Pooley, D. & Lewin, W. H. G. 2002, ApJ 578, 348.

Miller, J. M., Wojdowski, P., Schulz, N. S., Marshall, H. L., Fabian, A. C., Remillard, R. A., Wijnands, R., & Lewin, W. H. G. 2005, ApJ 620, 398.

Moffat, A. F. J. & Seggewiss, E. 1987, ESO Messenger No. 49, 26.

Moffat, A. F. J. & Shara, M. M. 1986, AJ 92, 952.

Moffat, A. F. J., Niemela, V. S., & Marraco, H. 1990a, ApJ 348, 232.

Moffat, A. F. J., Drissen, L., Robert, C., Lamontagne, R., Coziol, R., Mousseau, N., Niemela, V. S., Cerruti, M. A., Seggewiss, W., & van Weeren, N. 1990b, ApJ 350, 767.

Nadzhip, A. E., Khruzina, T. S., Cherepashchuk, A. M., & Shenavrin, V. I. 1996, Astron. Rep. 40, 338.

Nagae, O., Kawabata, K. S., Fukazawa, Y., Okazaki, A., & Isogai, M. 2008, AIPC 968, 328.

Natali, G., Fabrianesi, R. & Messi, R. 1978, 62, L1.

Niemela, V. S. 1982, IAU Symp 99, 299.

Niemela, V. S. 1995, IAU Symp 163, 223.

Niemela, V. S., Massey, P., & Conti, P. S. 1984, PASP 96, 549.

Niemela, V. S., Mandrini, C. H., & Méndez, R. H. 1985, Rev Mex Astron Astr 11, 143.

Ninkov, Z., Walker, G. A. H., & Yang, S. 1987a, ApJ 321, 425.

Ninkov, Z., Walker, G. A. H., & Yang, S. 1987b, ApJ 321, 438.

Nolt, I. G., Kemp, J. C., Rudy, R. J., Southwick, R. G., Radostitz, J. V., & Caroff, L. J. 1975, ApJ 199, L27.

Norton, A. J., Coe, M. J., Estela, A., Fabregat, J., Gorrod, M. J., Kastner, J., Payne, B. J., Reglero, V., Roche, P., & Unger, S. J. 1991, MNRAS 253, 579.

Özdemir, S. & Demircan, O. 2001, Astron. Space Sci 278, 319.

Paciesas, W. S., Robinson, C. R., McCollough, M. L., Zhang, S. N., Harmon, B. A., & Wilson, C. A. 1997, AIPC 410, 834.

Parsignault, D. R., Epstein, A., Grindlay, J., Schreier, E., Schnopper, H., Gursky, H., Brinkman, A. C., Heise, J., Schrijver, J., & Tanaka, Y. 1976a, Ap&SS 42, 175.

Parsignault, D. R., Grindlay, J. E., Schnopper, H., Schreier, E. J., & Gursky, H. 1976b, in *X-ray Binaries*, eds. E. Boldt & Y. Kondo. National Technical Information Service, Springfield, p. 429.

Phillips, K. C. & Mészáros, P. 1986, ApJ 310, 284.

Piirola, V. & Linnaluoto, S. 1988, in *Polarized Radiation of Circumstellar Origin*, ed. G. V. Coyne et al. Vatican Observatory, Vatican, p. 655.

Piirola, V., Berdyugin, A., Mikkola, S., & Coyne, G. V. 2005, ApJ 632, 576.

Pooley, G. G., Fender, R. P., & Brocksopp, C. 1999, MNRAS 302, L1.

Poutanen, J. 1998, in *Theory of Black Hole Accretion Discs*, eds. Abramowicz, M., Björnsson, G., Pringle, J. Cambridge Univ. Press, Cambridge, p. 100.

Poutanen, J., Zdziarski, A. A., & Ibragimov, A. 2008 arXiv:0802.1391v1 (P08).

Pravdo, S. H., White, N. E., Becker, R. H., Kondo, Y., Boldt, E. A., Holt, S. S., Serlemitsos, P. J., & McCluskey, G. E. 1980, ApJ 327, L71.

Priedhorsky, W. C., & Terrell, J. 1982, BAAS 14, 618.

Priedhorsky, W. C., Terrell, J., & Holt, S. S. 1983, ApJ 270, 233.

Priedhorsky, W. C., Brandt, S., & Lund, N. 1995, A&A 300, 415.

Pringle, J. E., & Rees, M. J. 1972, A&A 21, 1.

Remillard, R. A. & Canizares, C. R. 1984, ApJ 278, 761.

Robert, C., Moffat, A. F. J., Bastien, P., St.-Louis, N., & Drissen, L. 1990, ApJ 359, 211.

Roche, P., Larionov, V., Tarasov, A. E., Fabregat, J., Clark, J. S., Coe, M. J., Kalv, P., Larionova, L., Negueruela, I., Norton, A. J., & Reig, P. 1997, A&A 322, 139.

Rudy, R. J. & Herman, L. C. 1978, PASP 90, 163.

Rudy, R. J. & Kemp, J. C. 1978, ApJ 221, 200.

Russell, D. M., Fender, R. P., Gallo, E., & Kaiser, C. R. 2007, MNRAS 376, 1341.

Sculte-Ladbeck, R. E. & van der Hucht, K. A. 1989, ApJ 337, 872.

Seggewiss, W. 1974, A&A 31, 211.

Serkowski, K., Mathewson, D. S., & Ford, V. L. 1975, ApJ 196, 261.

Severny, A. B. & Kuvshinov, V. M. 1975, ApJ 200, L13.

Shakhovskoi, N. M. 1965, SvA 8, 833.

Shakura, N. I. & Syunyaev, R. A. 1973, A&A 24, 337.

Shapiro, S. L., Lightman, A. P., & Eardley, D. M. 1976, ApJ 204, 187.

Shaposhnikov, N. & Titarchuk, L. 2007, ApJ 663, 445 (ST07).

Simmons, J. F. L., Aspin, C., & Brown, J. C. 1980, A&A 91, 97 (S80).

Simmons, J. F. L., Aspin, C., & Brown, J. C. 1982, MNRAS 198, 45.

Sowers, J. W., Gies, D. R., Bagnuolo, W. G., Jr., Shafter, A. W., Wiemker, R., & Wiggs, M. S. 1998, ApJ 506, 424.

St.-Louis, N., Drissen, L., Moffat, A. F. J., & Bastien, P. 1987, ApJ 322, 870.

St.-Louis, N., Moffat, A. F. J., Drissen, L., Bastien, P., & Robert, C. 1988, ApJ 330, 286.

Stevens, I. R. 1991, ApJ 379, 310.

Stickland, D. J., Bromage, G. E., Budding, E., Burton, W. M., Howarth, I. D., Jameson, R., Sherrington, M. R., & Willis, A. J. 1984, A&A 134, 45.

Stirling, A. M., Spencer, R. E., de la Force, C. J., Garrett, M. A., Fender, R. P., & Ogley, R. N. 2001, MNRAS 327, 1273.

Sunyaev, R. A. & Titarchuk, L. G. 1985, A&A 143, 374.

Syunyaev, R. A. & Trümper, J. 1979, Nature 279, 506.

Titarchuk, L. & Fiorito, R. 2004, ApJ 612, 988 (TF04).

Villar-Sbaffi, A., St-Louis, N., Moffat, A. F. J., & Piirola, V. 2006, ApJ 640, 995.

Voloshina, I. B., Lyuty, V. M., & Tarasov, A. E. 1997, SvA 23, 3.

Walborn, N. R. 1973, ApJ 179, L123.

Walker, E. N. 1972, MNRAS 160, 9P.

Webster, B. L. & Murdin, P. 1972, Nature 235, 37.

Wen, L., Cui, W., Levine, A. M. & Bradt, H. V. 1999, ApJ 525, 968.

White, N. E., Kallman, T. R., & Swank, J. H. 1983, ApJ 269, 264.

Wilking, B. A., Lebofsky, M. J., Kemp, J. C., Martin, P. G., & Rieke, G. H. 1980, ApJ 235, 905.

Wolinski, K. G. & Dolan, J. F. 1994, MNRAS 267, 5 (WD94).

Wolinski, K. G., Dolan, J. F., Boyd, P. T., Biggs, J. D., Nelson, M. J., Percival, J. W., Taylor, M., & van Citters, G. W. 1996, ApJ 457, 859 (W96).

Zdziarski, A. A. & Gierliński, M. 2004, Prog. Theor. Phys. Suppl. 155, 99.

Zdziarski, A. A., Gierliński, M., Gondek, D., & Magdziarz, P. 1996, A&AS 120, 553.

Zdziarski, A. A., Johnson, W. N., Poutanen, J., Magdziarz, P., & Gierliński, 1997, in The Transparent Universe, Proc. 2nd INTEGRAL Workshop, eds. C. Winkler, T. J.-L. Courvoisier, & P. Durouchoux. ESA Publications Division, Noordwijk, p. 373.

Zhang, S. N., Robinson, C. R., & Cui, W. 1996, IAU Circ. 6510.

Ziólkowski, J. 2005, MNRAS 358, 851.